NOTICE: This is the author's version of a work that was accepted for publication in Journal of Geotechnical and Geoenvironmental Engineering. Changes resulting from the publishing process, such as peer review, editing, corrections, structural formatting, and other quality control mechanisms may not be reflected in this document. Changes may have been made to this work since it was submitted for publication. A definitive version was subsequently published in Journal of Geotechnical and Geoenvironmental Engineering, 148:11, 2022. doi: https://doi.org/10.1061/(ASCE)GT.1943-5606.0002906

Long-term response of piles to cyclic lateral loading following vibratory and impact driving in water-saturated sand

Patrick Staubach*; Jan Machaček†; Britta Bienen‡; Torsten Wichtmann§

Abstract: The influence of the pile installation by vibratory or impact driving on the response to subsequent cyclic lateral loading, as faced in the offshore environment, is investigated numerically. Large-deformation analyses of the pile installation process using the Coupled Eulerian-Lagrangian method considering partially drained conditions are performed. Following the installation, one million lateral load cycles are simulated using the high-cycle accumulation (HCA) model. The lower the hydraulic conductivity of the soil during driving, the higher the accumulation of lateral deformation when the pile is subjected to high-cyclic loading. The assumption of ideally drained conditions during pile driving results in a lower accumulation, in particular for the vibratory driven pile. Compared to the influence of the drainage conditions during driving, the influence of the installation method is found to be of less importance. While the vibratory driven piles tend to give less resistance to monotonic lateral loading for most conditions, slightly lower permanent pile head rotations after one million lateral loading cycles are observed compared to the impact driven piles.

Keywords: pile installation; vibratory driving; impact driving; high-cyclic loading; high-cycle accumulation model; large deformations

*Chair of Soil Mechanics, Foundation Engineering and Environmental Geotechnics, Ruhr Universität Bochum, Germany/Chair of Geotechnics, Bauhaus Universität Weimar, Germany. Email: patrick.staubach@uni-weimar.de, Corresponding author

†Institute of Geotechnics, Technische Universität Darmstadt, Germany/Chair of Soil Mechanics, Foundation Engineering and Environmental Geotechnics, Ruhr-Universität Bochum, Germany

‡Centre for Offshore Foundation Systems, Oceans Graduate School, University of Western Australia, Crawley, Perth, WA, Australia

§Chair of Soil Mechanics, Foundation Engineering and Environmental Geotechnics, Ruhr-Universität Bochum, Germany

1 Introduction

The installation of piles changes the state of the surrounding soil. It is known from experimental investigations that the pile response to loading following the installation process is influenced by the installation method (see e.g. (Dyson and Randolph, 2001; Anusic et al., 2019; Stein et al., 2020; Achmus et al., 2020; Fan et al., 2021b)).

Following their installation, piles are often subjected to cyclic lateral loading. Such loading conditions are very relevant for foundations of offshore wind turbines (OWTs), which are loaded by a large number of lateral loading cycles during their lifetime. Impact pile driving is the most widespread pile installation method for foundations of OWTs and thus there is extensive experience in driving and estimating the pile response to subsequent loading. High levels of (underwater) noise are emitted during the driving process (Henke et al., 2011; Göttsche et al., 2015; Tsouvalas, 2020), however, which can be problematic when installing offshore piles. For instance, the German Federal Environment Agency enforces a restriction of noise level to 190 dB for installation of offshore structures (UBA, 2011). Compared to impact driving, vibratory driving exhibits lower noise emissions. The cyclic movement of the pile during driving reduces the resistance in the soil such that the pile can be driven with relatively low static forces. Vibratory driving is often used in case of water-saturated soil or it is combined with impact driving in case the penetration resistance can not be overcome during the installation process. Vibratory driven piles are sometimes reported to have lower load capacity compared to impact driven or jacked piles (Grabe and Pucker, 2015; Achmus et al., 2020). In addition, vibratory driven piles are often reported to accumulate more deformation when subjected to cyclic lateral loading compared to impact driven piles (Labenski and Moormann, 2019; Stein et al., 2020). The lower resistance of vibratory driven piles (to subsequent vertical loading) is, for instance, also mentioned in the German guidelines for piles "EA Pfähle" (DGGT, 2012). Similarly, in The Overseas Coastal Area Development Institute of Japan (2002) it is recommended to perform the final phase of the vibratory driving process by impact driving in order to increase the base resistance of the pile.

Due to the lower noise emission, there is an increasing interest in the investigation of the applicability of vibratory driving and alternative driving methods, such as "Gentle Driving of Piles" (Tsetas et al., 2020) amongst others, for the installation of monopiles for OWTs. It is, however, yet unclear if the current design practices for the lateral loading of the foundation can be applied to vibratory driven piles since the methods applied are based on experience from impact driven piles.

A comparative numerical study of the influence of two installation techniques on the response of tubular open-ended piles to subsequent lateral loading with large numbers of cycles is presented in this work, considering piles with a low ratio $L/D = 2.5$ of pile length L to diameter D. For the simulation of the pile installation process, the Coupled Eulerian-Lagrangian method available in the software package `Abaqus` is used. It is extended to consider partially drained conditions, being very relevant for the installation of piles in water-saturated soils. Following the installation by vibratory or impact driving, the resulting soil state

is transferred to a purely Lagrangian model and the (high-cyclic) lateral loading of the pile is simulated using the high-cycle accumulation (HCA) model (Niemunis et al., 2005) implemented in the finite-element code `numgeo` (see e.g. (Machaček, 2020; Machaček et al., 2021; Staubach et al., 2022b; Staubach et al., 2022c) and www.numgeo.de) developed by the first two authors.

2 Soil mechanism during pile driving and influence of the pile installation process on its response to subsequent loading

2.1 Installation-induced changes in stress

The effects of pile driving on the state of the soil in the vicinity of the pile have so far been investigated primarily for jacking and impact driving. From experiments in dry sand it is known that the stress below the pile tip increases significantly and grain crushing can occur (Yang et al., 2010). Once the pile tip passes the soil, a sharp reduction of effective (radial) stress acting on the pile shaft was observed in experiments (White and Lehane, 2004; Yang et al., 2010; Jardine et al., 2013a; Burali d'Arezzo et al., 2015). A schematic of the development of the radial stress in the soil close to the pile shaft is given in Fig. 1a (based on White and Bolton (2004)).

With increasing distance h (measured from the pile tip directed to the ground surface), the radial stress tends to reduce further, which is known as *friction fatigue* (Heerema, 1978) or h/R effect (Bond and Jardine, 1991) (in some papers, the term h/R effect is used to describe a general change of the soil state with h, not necessarily a reduction of radial stress). A schematic of this phenomenon is given in Fig. 1b based on (Jardine et al., 2013b). The friction fatigue effect is more pronounced in case of cyclic shearing as occurring for vibratory pile driving. In general, cyclic interface shearing is observed to lead to larger contraction of the soil in the interface zone compared to monotonic shearing (DeJong et al., 2003; DeJong et al., 2006; Mortara and Mangiola, 2007).

The large increase in radial stress and the subsequent sharp reduction in the interface zone during the pile installation process are well visible from the results of a numerical simulation of the jacking of a pile in dry sand displayed in Fig. 1c. The simulations are documented in (Staubach et al., 2021c) and were performed using the Coupled Eulerian-Lagrangian (CEL) method. In addition, the friction fatigue effect is well visible in the plot on the far right.

Over time, the effective radial stress acting normal to the pile shaft, reduced by the installation process, may increase again. This phenomenon is referred to as *set-up* effect and is for instance described in (Chow et al., 1997; White and Bolton, 2004). The set-up effect is schematically shown in Fig. 1a.

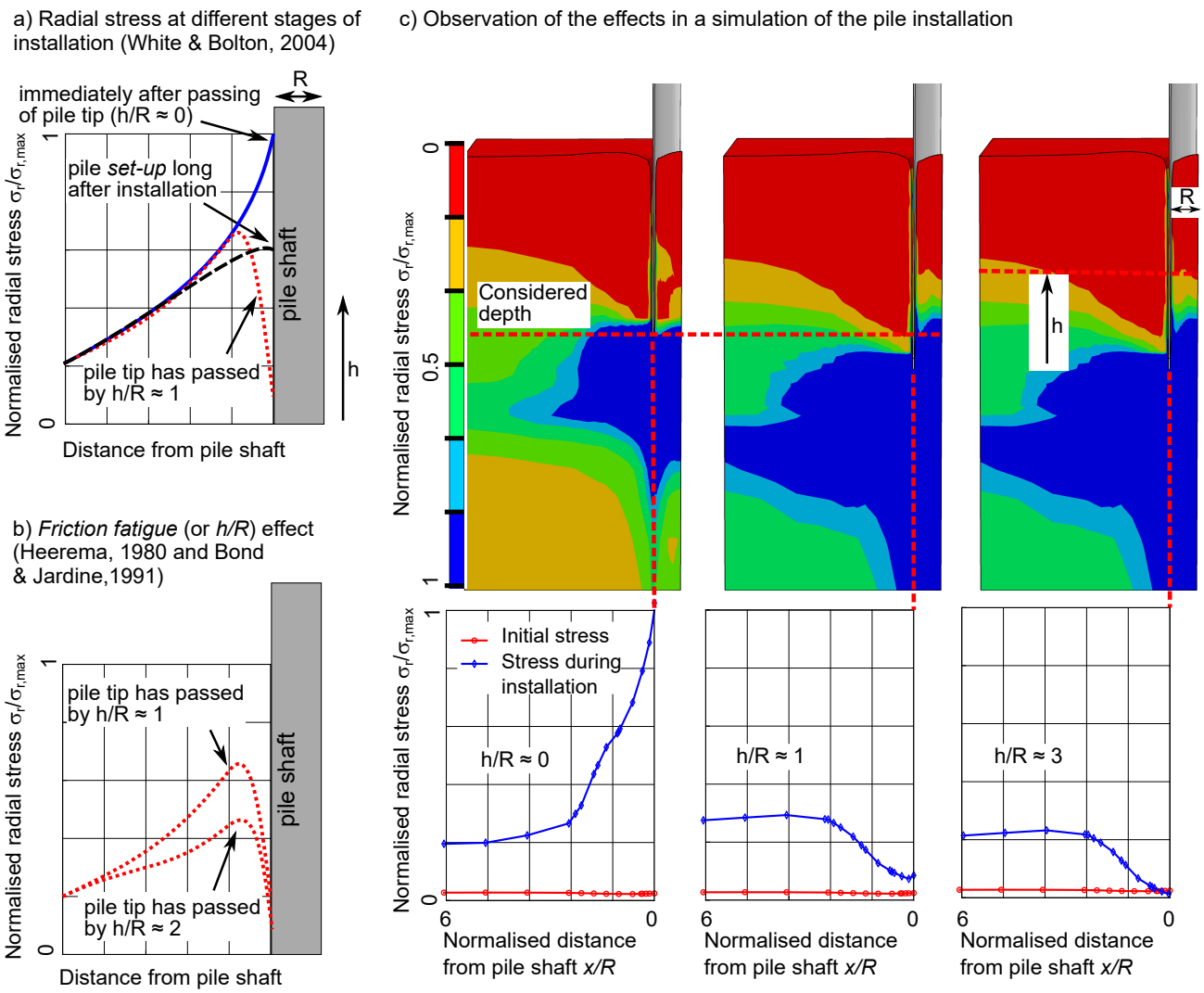

Fig. 1. a) Schematic of the development of effective radial stress acting in the soil in the vicinity of the pile shaft with respect to the distance h from the pile tip divided by the pile radius R (according to White and Bolton (2004)). b) Reduction of effective radial stress with ongoing pile penetration known as *friction fatigue* or h/R effect (according to Jardine et al. (2013b)). c) Effective radial stress distribution during a simulation of jacking of a pile in a small-scale model test set-up using the CEL method (x: distance from pile shaft). The distributions of radial stress at different times of the pile penetration process and at different depths are given (according to Staubach et al. (2021c)).

2.2 Response of vibratory driven piles to (cyclic) lateral loading

Recently, field tests to investigate the influence of the pile installation technique on the response to lateral loading have been performed in a test pit at the Institute of Geomechanics and Geotechnics at Braunschweig University (Stein et al., 2020). The piles had a diameter of 0.61 m and were driven 2.4 m in water-saturated sand with an initial relative density of approximately 70 %. The hydraulic conductivity of the sand was approximately $5 \cdot 10^{-4}$ m/s. Vibratory driving was either performed in a free-riding manner or crane-guided. In contrast to impact driven piles, for which an increase in effective radial stress in the vicinity of the pile tip was observed, the effective stress did not change as significantly for the crane-guided vibrated piles. However, piles vibrated in a free-riding manner showed similar increase in effective stress as the

impact driven piles. With regard to the monotonic lateral load behaviour, significant differences were found between impact driven and crane-guided vibrated piles. A stiffer response was observed for the impact driven pile. Furthermore, the impact driven pile showed lower accumulation of deformation under cyclic lateral loading compared to the crane-guided vibrated pile. Free-riding vibrated piles showed accumulated displacements in between those of impact driven and crane-guided vibrated piles. For all piles, a steady increase in the system stiffness with increasing number of lateral load cycles was observed. As a result of the cyclic lateral loading of the pile, stress redistribution occurred in the soil close to the pile. However, the increased radial stress close to the pile tip caused by the installation process by impact driving was still present after 10,000 lateral load cycles.

The results of Stein et al. (2020) agree with the results of another recent field test campaign conducted by Achmus et al. (2020), where the lateral load behaviour of vibrated piles was compared to impact driven piles. The subsoil at the test side close to Cuxhaven (Germany) consisted mainly of fine to medium coarse silica sands with medium dense to dense initial state. The water table was located 4.2 m below the ground surface. The piles had a diameter of 4.3 m and were driven to a depth of approximately 19 m. When subjected to monotonic lateral loading following the installation, piles driven with typical vibratory driving frequencies showed larger lateral deflection compared to the impact driven piles for the same lateral load magnitude.

In contrast to these studies, another recent field test campaign found that vibratory driven piles had a slightly higher resistance to lateral monotonic loading than impact driven piles (Anusic et al., 2019). It was hypothesised that the higher resistance was due to greater compaction of the soil caused by vibratory driving. In these tests, the soil consisted of medium dense unsaturated sand. Similarly to the results of these field tests, vibratory driven piles in a small-scale 1g model test set-up with water-saturated dense sand showed a comparable behaviour to cyclic lateral loading for a number of load cycles larger than 10 (Hoffmann et al., 2020) or even a lower accumulation of deformations compared to impact driven piles (Le et al., 2021).

The numerical study carried out in this work aims to shed some light on these contradictory trends. In contrast to existing numerical studies, different drainage conditions are considered, which is, in addition to the specifications of the pile driver, probably one of the key aspects to explain the observed different trends in lateral loading response originating from the installation technique.

3 Numerical simulation of the installation process

A numerical method able to model large-deformations is required for the analysis of pile installation processes. Simulations using the Coupled Eulerian-Lagrangian (CEL) method (Qiu et al., 2011; Henke, 2014; Hamann et al., 2015; Fan et al., 2021c; Bienen et al., 2021), the (Multi-Material) Arbitrary Lagrangian Eulerian method (Liyanapathirana, 2009; Tolooiyan and Gavin, 2011; Dijkstra et al., 2011; Aubram et al., 2015; Yang et al., 2020), the Material Point Method (Phuong et al., 2014; Hamad, 2016; Ceccato and

Simonini, 2017; Giridharan et al., 2020; Martinelli and Galavi, 2021), the Particle FEM (Hauser and Schweiger, 2021; Monforte et al., 2021; Zhang et al., 2021), the Discrete Element Method (Ciantia et al., 2016; Li et al., 2019) and the Smoothed Particle Hydrodynamics method (Cyril et al., 2019) are reported in the literature. A discussion of the different methods as well as of their advantages and disadvantages in applications to geotechnical boundary value problems is out of the scope of this work. The interested reader is referred to e.g. (Bojanowski, 2014; Wang et al., 2015; Soga et al., 2016; Augarde et al., 2021). In an Eulerian analysis the finite element mesh is technically fixed and the material moves through it. Therefore, the elements are not necessarily completely occupied by material. An Eulerian approach is of advantage if large deformations are modelled since no mesh distortion occurs. A numerical scheme in which both Lagrangian and Eulerian elements exist simultaneously and the contact between them is taken into account is called Coupled Eulerian-Lagrangian (CEL) method (Benson, 1992). In the finite element code `Abaqus` the CEL method is implemented employing an explicit central difference time integration scheme. The CEL method is appealing in particular for the simulation of pile driving, where the pile is modelled using a Lagrangian description and the soil, undergoing large deformations, is modelled in an Eulerian framework. Successful applications of the CEL approach in geomechanics have been reported e.g. in (Qiu et al., 2011; Andresen and Khoa, 2013; Wang et al., 2015; Heins and Grabe, 2017). However, with the built-in CEL method, only perfectly drained or perfectly undrained conditions can be considered. The extension of the CEL method implemented in `Abaqus` allowing for partially drained analysis of water-saturated soils utilised in the simulations presented in the following is based on the work reported in (Hamann et al., 2015; Hamann, 2015; Staubach et al., 2020b; Staubach et al., 2021b). A **u**-p element formulation (Zienkiewicz and Shiomi, 1984), discretising the displacement of the solid phase and the pore water pressure, is employed. For this purpose, the similarity of the energy balance and the mass balance of fluids is exploited. A thermally coupled analysis is performed, but the temperature is reinterpreted as excess pore water pressure. Note that the shortcoming of this approach regarding the incorporation of soil-structure interface friction, where it was not possible to distinguish between effective and total normal contact stresses as reported in (Staubach et al., 2020b; Staubach et al., 2021b), can be circumvented to some extent. For this purpose, the friction coefficient is defined as temperature-dependent, reducing with increasing excess pore water pressure. Details on this procedure can be found in (Staubach, 2022). Note in addition that cavitation is accounted for, such that the pore water pressure relative to the atmospheric pressure can not become lower than -100 kPa. A height of the water table of 10 m above the ground level is assumed.

The feasibility of the utilised hydro-mechanically coupled CEL method for the analysis of vibratory pile driving in water-saturated sand has been demonstrated by the authors in (Staubach et al., 2021b) by back-analysis of model tests and by comparison with simulations using a "conventional" **u**-p element formulation in the fully Lagrangian framework. Note that the **u**-p element formulation neglects the relative acceleration between solid grains and water, relevant for analyses with high wave frequencies f and high values of hydraulic conductivity k^w (Zienkiewicz et al., 1980; Simon et al., 1986; Navas et al., 2021;

Argani and Gajo, 2021). Both criteria are simultaneously met for the analysis of vibratory pile driving in sandy soils. Therefore, preliminary investigations of the simulation of vibratory pile driving using the **u**-p-**U** and **u**-**U** element formulation, both considering the relative acceleration, reported in (Staubach and Machaček, 2019), were conducted. The relative acceleration was found to be of little importance, justifying the application of the **u**-p element formulation for the analysis of vibratory pile driving in soils with high values of hydraulic conductivity (up to $k^w \approx 10^{-3}$ m/s with a frequency of $f \approx 50$ Hz). For lower values of hydraulic conductivity even for very large frequencies of $f > 100$ Hz no influence resulting from the negligence of relative acceleration is expected.

3.1 Numerical model

The numerical model is depicted in Fig. 2. A pile with a diameter of $D = 4$ m and a wall thickness of $t = 0.08$ m is driven 10 m in homogeneous sand. The soil is discretised using Eulerian elements while the pile, being assumed rigid without considering any intrinsic deformations, is modelled with conventional Lagrangian elements. In order to avoid artificial reflections of outwards travelling waves at the fixed boundaries of the model, a distance of 80 m ($= 20D$) from the pile to the outer boundary and a height of the model of 200 m ($= 50D$) are chosen. The node-to-node distances increase with increasing distance from the pile, leading to a progressive loss of higher frequency waves. Application of viscous dampers at the fixed borders could be an alternative approach, but `Abaqus` does not support parallelisation of the entire simulation process if such (built-in) boundary conditions are chosen. As can be seen from the field of acceleration on the right-hand side of Fig. 2, the waves caused by the pile installation do not reach the fixed boundaries of the model, since they are either dissipated by plasticity (material damping), geometrical damping or by the increasing distance between nodes. Therefore, the results of the simulations are not altered by artificial reflections. Since the installation process can lead to a heave of the soil surrounding the pile, an additional, initially material-empty, volume above the seabed is considered which can be filled by material during the installation process (red area in Fig. 2). The top surface of the soil allows for drainage during the installation. Note that once elements are no longer filled with material, no water flow through these elements is possible. Since the soil around the pile settles during driving, no drainage would be possible alongside this newly formed material boundary. Therefore, a constant pore water pressure is assigned for the top 0.3 m to allow for drainage even if the soil surface around the pile moves downwards.

The size of the soil elements in the vicinity of the pile is chosen equal to the wall thickness of the pile, such that the pile occupies exactly one Eulerian element across its wall section as it penetrates the soil. The required element size in relation to the size of the pile to ensure an accurate solution is determined by experience from previous simulations of the vibratory pile driving process using the CEL method reported in (Staubach et al., 2021b). The time increment is chosen to be identical to the critical time increment defined by the Courant-Friedrichs-Levy condition. During the simulation, this results in a time increment of approximately 10^{-4} s.

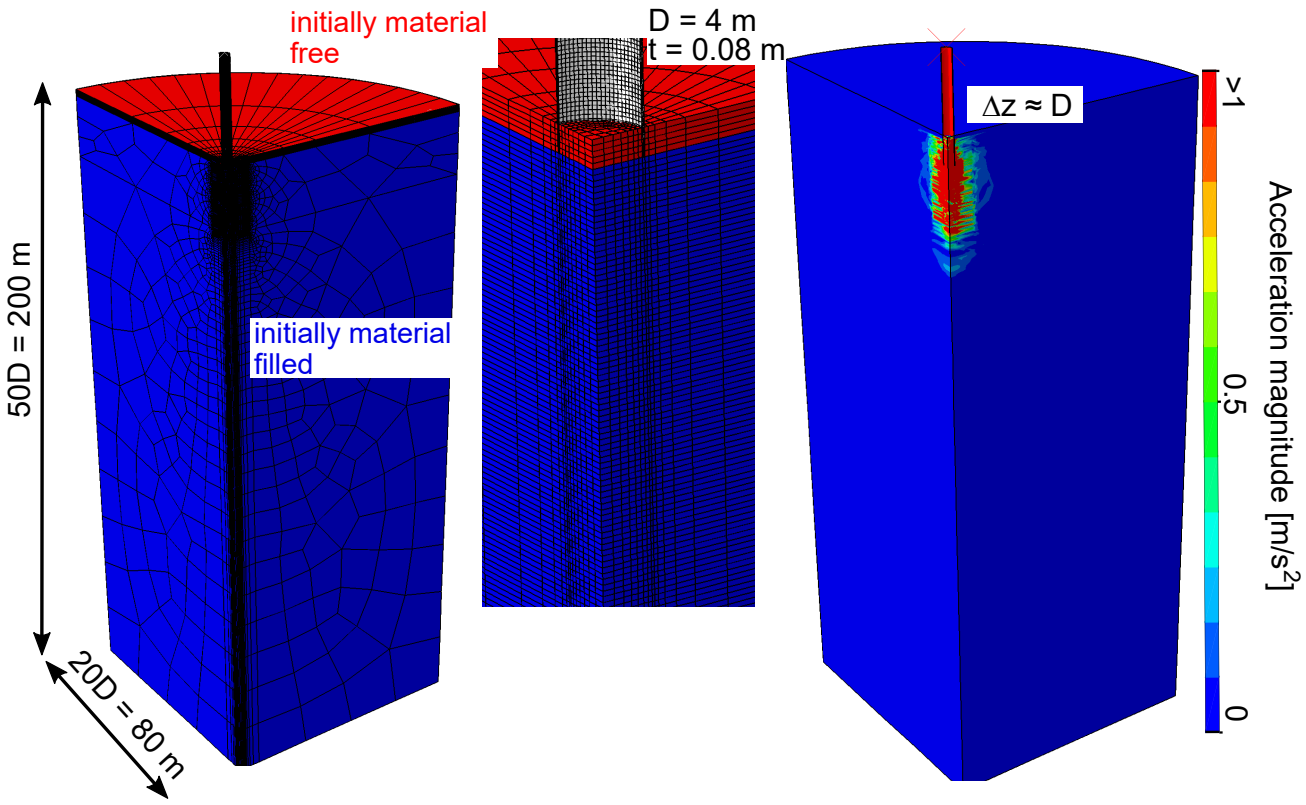

Fig. 2. Model for the simulation of the pile installation process and spatial distribution of the acceleration magnitude (gravity is subtracted) during the driving process at a pile penetration of approximately $\Delta z = D$

The soil is assumed to be "Karlsruhe fine sand". The hypoplastic model (Wolffersdorff, 1996) with intergranular strain extension (Niemunis and Herle, 1997) with parameters given in Table 1 is used. Initially medium dense ($D_{r0} = 50$ %) and dense soil conditions ($D_{r0} = 70$ %) are considered. The focus of the study is on the initially dense conditions, since it is the practically more relevant case for the offshore environment. The applied driving forces are chosen such that the penetration rate of the pile is comparable for both installation techniques and that the targeted final embedment depth can be achieved within a reasonable computational time. Note that compared to the pile installation process of monopiles in reality, for which the driving process may involve tens of thousands of hammer blows, only a limited number can be numerically simulated. A vibratory driving frequency of 30 Hz and an amplitude (single) of 1200 kN is set (all values for a full pile). The impact driving frequency is 0.65 Hz and the load magnitude 2400 kN. The impact force is active for 10 ms. In addition to the pile weight, a static load resulting from the driver and an additional extension of the pile, which is not modelled explicitly, of 2000 kN is considered for both installation techniques. The chosen specifications are typical values for vibratory drivers and hydro-hammers used by the industry.

Frictional contact between pile and soil is modelled using the standard Coulomb model with a friction coefficient of 0.5, which is a value typically found for surfaces of piles used for offshore foundations (Randolph and Gourvenec, 2017).

An isotropic hydraulic conductivity of $k^w = 10^{-3}$ m/s is assumed as the reference case. Additional

φ_c [-]	e_{i0} [-]	e_{c0} [-]	e_{d0} [-]	h_s [MPa]	n [-]	α [-]	β [-]	R [-]	m_R [-]	m_T [-]	β_R [-]	χ [-]
33.1°	1.212	1.054	0.677	4000	0.27	0.14	2.5	10^{-4}	2.4	1.2	0.1	6.0

Table 1. Parameters of the hypoplastic model with intergranular strain extension for "Karlsruhe fine sand"

simulations assuming ideally drained conditions (i.e. water-saturated conditions but perfect drainage), ideally undrained conditions (i.e. water-saturated conditions but no drainage) or a hydraulic conductivity of $k^w = 10^{-4}$ m/s are performed as well.

To evaluate the drainage conditions during driving, the dimensionless factor Π_1 introduced by Zienkiewicz et al. (1980) is used. It is defined by

$$\Pi_1 = \frac{k^w v_c^2 \rho^{\mathrm{tot}}}{g \rho^w \omega l^2}. \tag{1}$$

Therein the *characteristic length* l, the hydraulic conductivity k^w, the gravity $g = 10$ m/s^2, the angular frequency ω, the total density ρ^{tot}, the density of the water $\rho^w = 1$ t/m^3 and the compression wave velocity v_c of the soil-water mixture are used. The characteristic length l is the thickness of the soil layer considered in the analytical approach by Zienkiewicz et al. (1980) and is assumed to be identical to the embedded pile length of 10 m in the present case. The compression wave velocity is $v_c = 1700$ m/s and the total density $\rho^{\mathrm{tot}} = 1.86$ t/m^3. The values obtained for Π_1 for the different pile installation simulations are summarised in Table 2. In addition, the drainage conditions according to the diagram provided by Zienkiewicz et al. (1980) are given. Note that in (Zienkiewicz et al., 1980) values of $\Pi_1 < 10^{-2}$ are regarded to allow for the assumption of ideally undrained conditions, while values larger than 10^2 are considered to result in ideally drained conditions. In between, the response is considered to be partially drained. Since the (static) load magnitude is not considered in Π_1, the conditions given in Table 2 might not realistically reflect the actual conditions. However, it is believed that the evaluation of Π_1 at least allows to compare the drainage conditions between the different installation techniques. From Table 2 it is evident that the vibratory driving process leads to nearly undrained conditions, while for the impact driven pile at least for the higher value of hydraulic conductivity a larger influence by the consolidation process is expected. The conditions for the vibratory driven pile with $k^w = 10^{-3}$ m/s are similar to the impact driven pile with $k^w = 10^{-4}$ m/s, even though in case of the vibratory driven pile less influence from the consolidation process is expected.

3.2 Results of the simulations of the pile installation process

The pile penetration vs. time of driving plot for the vibratory driven piles is given in the left plot of Fig. 3 for different values of hydraulic conductivity and drainage conditions. Only the results of simulations with initially dense soil conditions ($D_{r0} = 70$ %) are shown. Due to numerical instabilities towards the end

Simulation	Π_1	Drainage conditions
VD ($k^w = 10^{-3}$ m/s)	0.028	nearly undrained
VD ($k^w = 10^{-4}$ m/s)	0.003	undrained
ID ($k^w = 10^{-3}$ m/s)	0.131	partially drained
ID ($k^w = 10^{-4}$ m/s)	0.013	nearly undrained

Table 2. Drainage conditions for the different pile installation simulations (VD: Vibratory Driving; ID: Impact Driving) using the dimensionless factor Π_1 and the diagram provided in (Zienkiewicz et al., 1980)

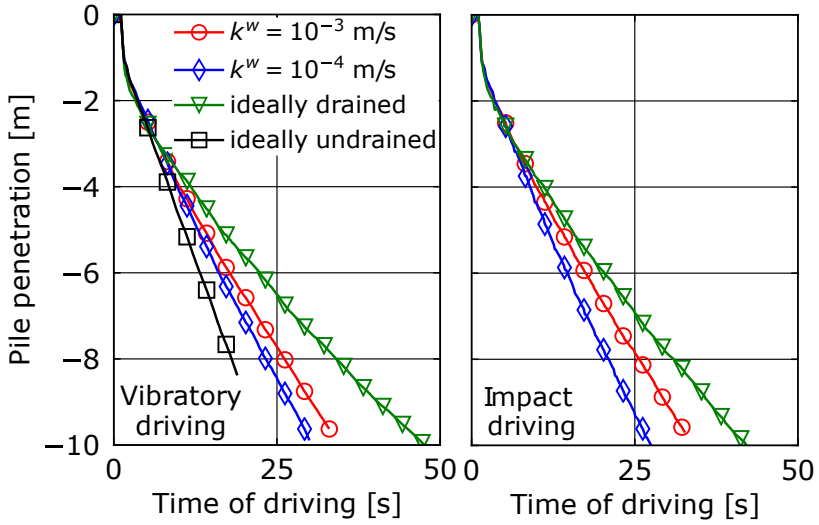

Fig. 3. Pile penetration vs. time of driving assuming different values of hydraulic conductivity k^w for vibratory driving (left plot) and impact driving (right plot)

of the simulation, the target embedment depth of 10 m was not reached in all cases. Approximately 30 cm are missing for the simulations with a hydraulic conductivity of $k^w = 10^{-3}$ m/s for both installation techniques.

As expected, the lower the hydraulic conductivity, the higher is the penetration rate. The assumption of ideally drained conditions leads to lower penetration rates, since no reduction of the soil strength due to a loss of effective stress occurs. For perfectly undrained conditions the highest penetration rate is observed for vibratory pile driving. Full liquefaction of the soil close to the pile occurs, which causes numerical problems and an abortion of the simulation before the targeted pile penetration depth is achieved. Therefore, the results of the ideally undrained simulations are not further evaluated in the following sections.

The influence of the hydraulic conductivity and the drainage conditions on the pile penetration rate is quantitatively and qualitatively similar for the impact driven piles, as can be seen from the right plot of Fig. 3. Given the chosen specifications of the pile drivers, for identical drainage conditions, the impact driven piles show a slightly faster penetration compared to vibratory driven piles. For the ideally drained simulations, nearly 1500 cycles of the vibrator are required to achieve an embedment depth of 10 m, whereas approximately 27 strokes are needed in case of impact driving. The difference in number of cycles experienced by the soil needs to be borne in mind for the results discussion.

The spatial distributions of effective radial stress, excess pore water pressure and relative density for

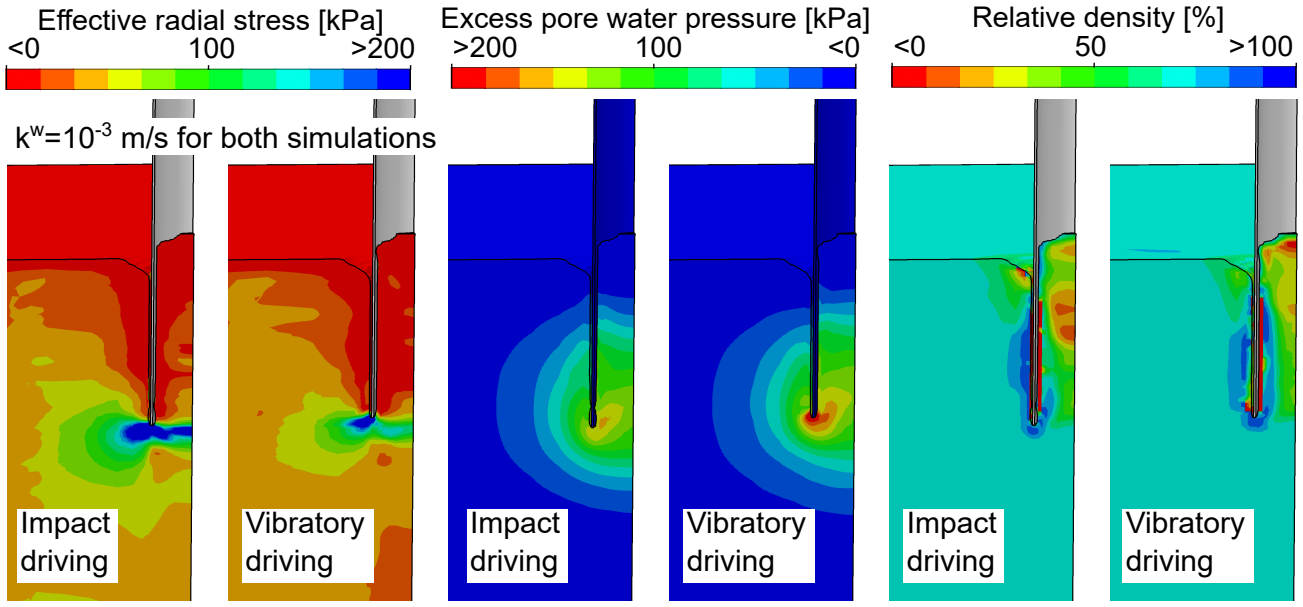

Fig. 4. Spatial distributions of effective radial stress, excess pore water pressure and relative density at a pile penetration depth of 10 m using impact and vibratory pile driving, respectively

impact and vibratory driving using a hydraulic conductivity of $k^w = 10^{-3}$ m/s are depicted in Fig. 4. Note that the geotechnical sign convention is used for the effective radial stress and only the simulations with initially dense soil conditions ($D_{r0} = 70$ %) are considered. Large values of effective stress in the vicinity of the pile tip are observed for both installation techniques. With increasing distance h from the pile tip (directed to the ground surface), the effective radial stress reduces drastically and reaches values lower than the effective radial stress prior to the installation. As visible in Fig. 4, the vibratory driven pile shows a somewhat lower increase in effective stress below the pile tip compared to the impact driven pile, due to larger excess pore water pressure. While the area of soil showing large excess pore water pressure is similar for both installation techniques, the magnitudes are larger in the vicinity of the pile tip for the vibratory driven pile. The spatial distribution of relative density shows that compaction of the soil close to the outer pile shaft occurs for both installation techniques. In addition, compaction below the pile tip is observed. In contrast, very loose states are reached in the soil close to the inner pile shaft for both installation methods. Compared to the vibratory driven pile, the compacted soil volume at the outer shaft is larger for the impact driven pile, which is most relevant for the response of the pile to subsequent lateral loading. However, a higher degree of compaction is observed inside the pile in case of vibratory driving.

The fields of effective radial stress and relative density for the ideally drained simulations are given in Fig. 5. Compared to the distributions obtained from the partially drained simulations provided in Fig. 4, the effective radial stress in the vicinity of the pile tip is much larger. In line with this observation the soil inside the pile does not heave as is observed in Fig. 4. Again, the vibratory driven pile shows a smaller increase in effective radial stress in the soil close to the pile tip, but the differences between the installation methods are much less pronounced than in case of the partially drained conditions. Similar to the partially drained simulations the radial stress is reduced at the pile shaft once the pile tip has passed the soil.

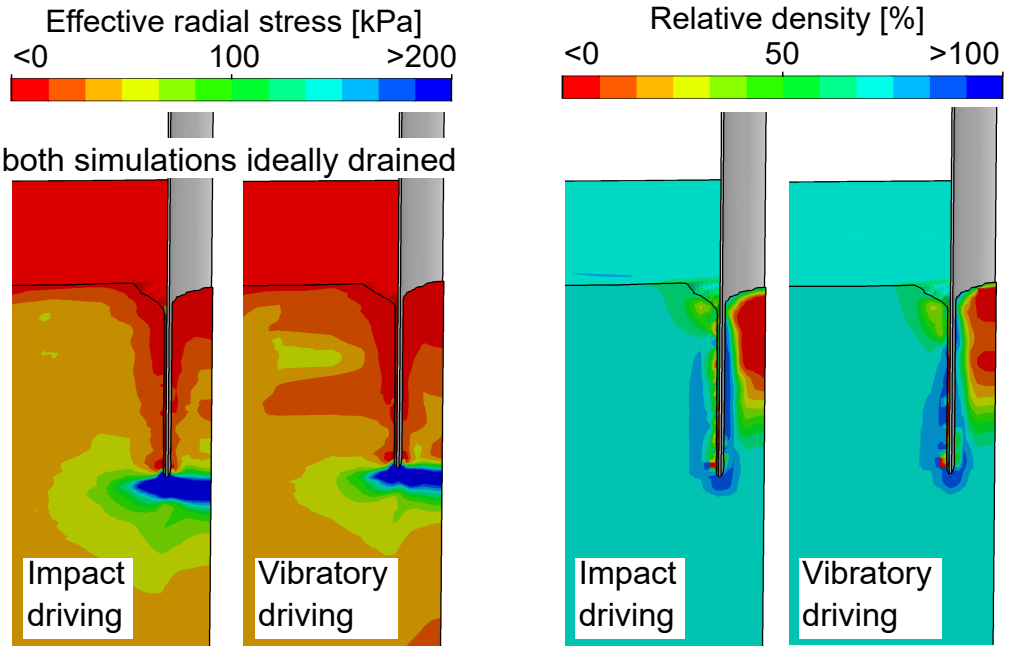

Fig. 5. Spatial distributions of effective radial stress and relative density at a pile penetration depth of 10 m using impact and vibratory pile driving, respectively. Ideally drained conditions are assumed.

For both installation techniques the compaction of the soil close to the pile tip is slightly more pronounced for the ideally drained conditions compared to the simulations assuming a hydraulic conductivity of $k^w = 10^{-3}$ m/s. In contrast to the partially drained simulations, no loosening of the soil close to the pile shaft inside the pile occurs. The soil inside the pile close to the axis of symmetry shows a strong reduction of relative density for both pile installation techniques, which is more pronounced for the ideally drained conditions compared to the partially drained case. In addition, much higher effective radial stresses develop inside of the pile close to the pile tip in case of ideally drained conditions, indicating a (partially) plugged state. Therefore, despite the greater loosening of the soil close to the ground surface inside the pile in case of ideally drained conditions, less heaving of the soil occurs inside the pile compared to the simulation assuming a hydraulic conductivity of $k^w = 10^{-3}$ m/s.

The spatial distributions for the installation using a hydraulic conductivity of $k^w = 10^{-4}$ m/s are depicted in Fig. 6. As expected, the consideration of a lower hydraulic conductivity leads to larger excess pore water pressures and less compaction of the soil near the pile tip. Somewhat surprisingly, the effective radial stress in greater distance from the pile shaft is larger for both installation techniques compared to the simulations using a hydraulic conductivity of $k^w = 10^{-3}$ m/s given in Fig. 4. This is due to the development of negative excess pore water pressure in greater distance from the pile shaft, increasing the effective stress. This negative excess pore water pressure is discussed later in more detail on the basis of Fig. 8.

The distribution of effective radial stress and excess pore water pressure with distance to the (outer) pile shaft for a depth of 5 m is given for different values of h/R (see Section 2) in Fig. 7. Since the depth is constant, the elements or nodes for which the quantities are evaluated do not change. The results from the

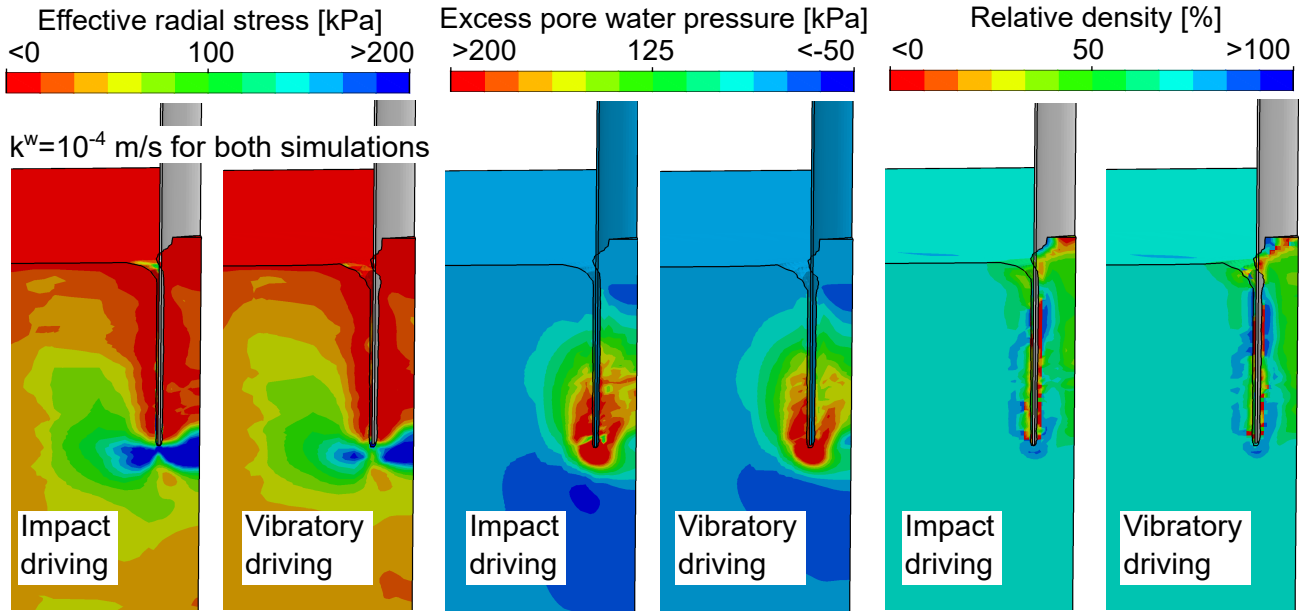

Fig. 6. Spatial distributions of effective radial stress, excess pore water pressure and relative density at a pile penetration depth of 10 m using impact and vibratory pile driving, respectively. A hydraulic conductivity of $k^w = 10^{-4}$ m/s is assumed.

simulations using a hydraulic conductivity of $k^w = 10^{-3}$ m/s for both installation techniques are shown. At passing of the pile tip ($h/R = 0$), the effective radial stress increases significantly for both installation techniques. Values larger than the initial effective radial stress are reached even for a distance from the pile of 5 m. The vibratory driven pile shows slightly lower values of effective radial stress and higher values of excess pore water pressure compared to the impact driven pile. Once the pile has passed the soil by 1 m ($h/R = 0.5$), a sharp reduction of effective radial stress nearby the pile occurs, while the excess pore water pressure remains nearly unchanged. Effective radial stress values close to zero are observed in the vicinity of the pile shaft for both installation techniques. This effect has been discussed in Section 2 and is well known from experimental studies (performed mostly in dry sand, however). To date, this effect has not been investigated in detail for vibratory driven piles in water-saturated sand. In addition, to the authors' best knowledge, no experimental study considering water-saturated and realistic stress conditions has investigated by local stress measurements if the h/R effect is quantitatively comparable for the two installation techniques.

The simulations indicate that the h/R effect is qualitatively similar for impact and vibratory driven piles. In case of the impact driven pile, larger effective radial stress is observed at $h/R = 0.5$ compared to the vibratory driven pile. However, for $h/R = 1$, both installation techniques show similar values of effective radial stress. The comparison of the stress at $h/R = 0.5$ with $h/R = 1$ shows that both installation techniques lead to a reduction of effective radial stress in the soil close to the pile shaft with increasing distance from the pile tip, i.e. the h/R effect. Interestingly, the effect is found to be quantitatively very similar for both installation techniques, considering the change in effective radial stress from $h/R = 0$ to $h/R = 1$. However, comparing the distributions of $h/R = 0$ with $h/R = 0.5$, the general consensus that

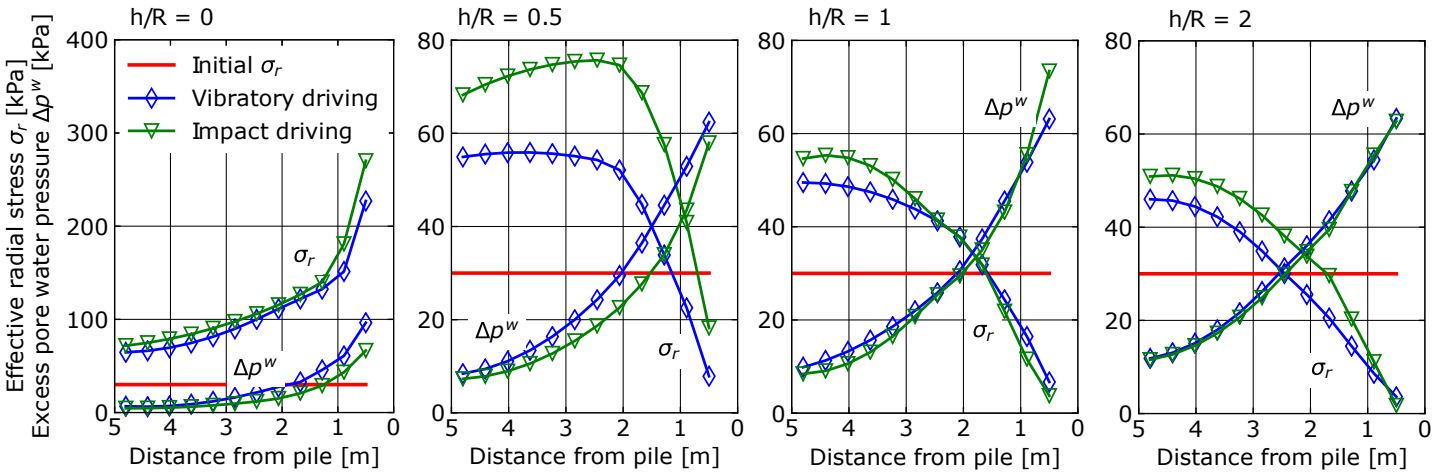

Fig. 7. Effective radial stress and excess pore water pressure vs. radial distance from the pile in a depth of 5 m at different values of h/R for impact and vibratory driving, respectively. A hydraulic conductivity of $k^w = 10^{-3}$ m/s is used in both cases.

the cyclic shearing exerted by vibratory driving leads to a stronger reduction in effective radial stress with increasing value of h/R compared to impact driving is confirmed. This is due to the stronger contractancy of the soil during (high-)cyclic interface shearing, as has been discussed previously. The distribution of the effective radial stress at $h/R = 2$ confirms the stronger stress reduction in case of vibratory driving. While the effective radial stress in case of the vibratory driven pile reduces further, the stress in case of the impact driven pile is not changed considerably compared to the distribution at $h/R = 1$.

To examine the influence of the hydraulic conductivity on the distribution of effective radial stress and excess pore water pressure with distance to the (outer) pile shaft, the results for vibratory driving using a hydraulic conductivity of $k^w = 10^{-3}$ m/s and $k^w = 10^{-4}$ m/s are compared in Fig. 8. For every vertical distance from the pile tip h/R the excess pore water pressure close to the pile is much larger for $k^w = 10^{-4}$ m/s compared to $k^w = 10^{-3}$ m/s. However, at a greater horizontal distance $> 1 - 3$ m from the pile shaft, the excess pore water pressure is less for $k^w = 10^{-4}$ m/s compared to $k^w = 10^{-3}$ m/s for every value of h/R, reaching even negative values. With increasing value of h/R the distance from the pile tip at which the lower hydraulic conductivity results in less excess pore water pressure increases and is approximately 2.5 m for $h/R = 2$. In line with the lower value of excess pore water pressure, the effective radial stress is larger for $k^w = 10^{-4}$ m/s for greater distances from the pile shaft compared to $k^w = 10^{-3}$ m/s. This has already been observed from the spatial distribution of effective radial stress given in Fig. 6, where larger values of effective stress than in Fig. 4 are visible in greater distance to the pile shaft. Close to the pile shaft, similar values of effective radial stress are observed for both values of hydraulic conductivity independent of h/R. Very low values of radial effective stress are reached, indicating a complete loss of soil stiffness. Compared to the change of effective radial stress with h/R, the excess pore water pressure shows much less change for values of $h/R > 0.5$, in particular for the lower value of k^w. In greater distance from the pile shaft, the h/R effect is stronger for the simulation with a lower value of hydraulic conductivity since the increase in effective radial stress and subsequent drop once the pile has passed the soil in the

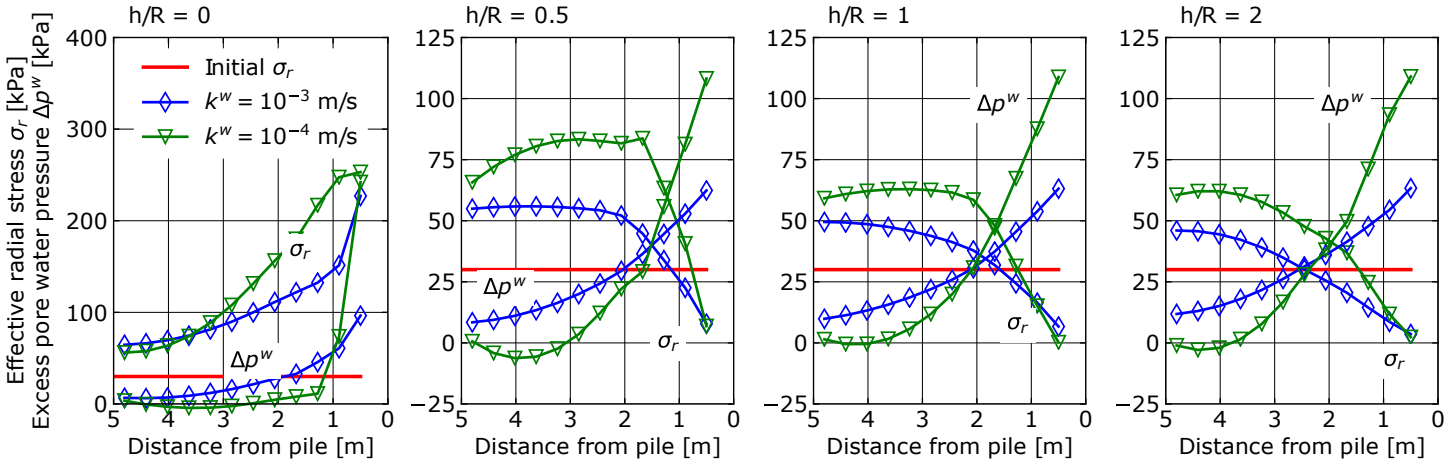

Fig. 8. Effective radial stress and excess pore water pressure vs. radial distance from the pile in a depth of 5 m at different values of h/R for vibratory driving using a hydraulic conductivity of $k^w = 10^{-3}$ m/s and $k^w = 10^{-4}$ m/s, respectively

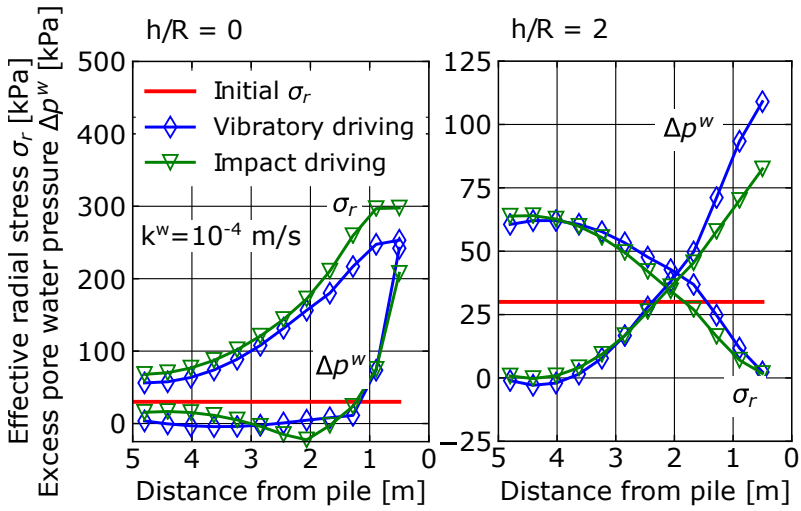

Fig. 9. Effective radial stress and excess pore water pressure vs. radial distance from the pile in a depth of 5 m at different values of h/R for impact and vibratory driving, respectively. A hydraulic conductivity of $k^w = 10^{-4}$ m/s is used in both cases.

considered depth is much larger compared to the higher hydraulic conductivity. However, considering the larger excess pore water pressure of the simulation with $k^w = 10^{-4}$ m/s, the final stress distributions once the driving has stopped and consolidation is finished are estimated to be comparable.

Fig. 9 compares the distributions of effective radial stress and excess pore water pressure for a hydraulic conductivity of $k^w = 10^{-4}$ m/s for vibratory and impact driven piles. Values for $h/R = 0$ and $h/R = 2$ in a depth of 5 m are evaluated. As observed for $k^w = 10^{-3}$ m/s, vibratory driving leads to higher peak values of excess pore water pressure and lower effective radial stresses compared to impact driving for $h/R = 0$. However, even for $h/R = 2$, in contrast to the simulation with higher value of k^w, the excess pore water pressure during impact driving is considerably lower close to the pile shaft than for vibratory driving. Despite this, lower values of effective radial stress are observed for $h/R = 2$ in the case of impact driving in a distance of 1-3 m from the pile shaft.

The main findings from the simulations of pile installation can be summarised as follows:

- Considering partially drained conditions with a hydraulic conductivity of $k^w = 10^{-3}$ m/s, the impact driven piles show a slightly larger increase in effective radial stress compared to the vibratory driven piles. In addition, a slightly stronger compaction in the vicinity of the pile tip occurs.
- Assuming ideally drained conditions, the opposite tendencies are observed for the change in relative density, i.e. the vibratory driven pile leads to a slightly higher compaction near the pile tip.
- Both installation techniques exhibit the h/R effect (i.e. reduction of effective radial stress with increasing distance h from the pile tip), being more pronounced for a lower value of hydraulic conductivity. The reduction of radial effective stress in the soil following the passing of the pile tip is slightly more pronounced for the vibratory driven pile in case of a hydraulic conductivity of $k^w = 10^{-3}$ m/s.

4 High-cyclic lateral loading following the installation process

4.1 The HCA model

In order to take into account millions of loading cycles such as encountered for offshore foundations, the high-cycle accumulation (HCA) model by Niemunis et al. (2005) has proven suitable in many previous studies (Machaček et al., 2018; Zachert et al., 2020; Zachert, 2015; Wichtmann et al., 2018; Staubach et al., 2020b; Staubach and Wichtmann, 2020; Staubach et al., 2021a; Staubach et al., 2020a; Jostad et al., 2020; Page et al., 2021; Le et al., 2021; Staubach et al., 2022a). In contrast to conventional constitutive models, the HCA model does not predict the material response during individual cycles but only the trend of stress and strain, allowing consideration of a large number of cycles during a calculation increment. As input the HCA model requires the cyclic strain amplitude, retrieved from the strain path of an individual load cycle, calculated using a conventional constitutive model (e.g. the hypoplastic model or the Sanisand (Dafalias and Manzari, 2004) model, see e.g. Staubach et al. (2022a)). Usually, two individual load cycles are simulated using the conventional constitutive model of which the second cycle is used to record the strain path, from which the strain amplitude is calculated. A multi-dimensional definition of the strain amplitude is used, which can be found in (Niemunis et al., 2005).

The basic equation of the HCA model reads (Niemunis et al., 2005):

$$\dot{\boldsymbol{\sigma}} = \mathsf{E} : (\dot{\boldsymbol{\varepsilon}} - \dot{\boldsymbol{\varepsilon}}^{\mathrm{acc}} - \dot{\boldsymbol{\varepsilon}}^{\mathrm{pl}}) \tag{2}$$

with the effective stress rate $\dot{\boldsymbol{\sigma}}$, the strain rate $\dot{\boldsymbol{\varepsilon}}$, the accumulation rate $\dot{\boldsymbol{\varepsilon}}^{\mathrm{acc}}$, a plastic strain rate $\dot{\boldsymbol{\varepsilon}}^{\mathrm{pl}}$, which is non-zero only if the effective stress reaches the Matsuoka-Nakai failure locus, and the pressure-dependent elastic stiffness E. In Eq. (2), the dot over a symbol means a derivative with respect to the number of

cycles N, i.e. $\dot{\sqcup} = \partial \sqcup / \partial N$. The key aspect of the model is the accumulation rate $\dot{\boldsymbol{\varepsilon}}^{\text{acc}}$, which is calculated by

$$\dot{\boldsymbol{\varepsilon}}^{\text{acc}} = f_{\text{ampl}}\ \dot{f}_N\ f_e\ f_p\ f_Y\ \mathbf{m}, \tag{3}$$

where $\mathbf{m} = (\dot{\boldsymbol{\varepsilon}}^{\text{acc}})^{\rightarrow}$ is the *direction* of strain accumulation. The scalar factors consider the influence of the strain amplitude $\varepsilon^{\text{ampl}}$ (function f_{ampl}), the cyclic preloading ($\dot{f}_N$), the void ratio e (f_e), the average mean pressure p^{av} (f_p) and the normalised average stress ratio $\bar{Y}^{\text{av}}$ (f_Y, $\bar{Y}^{\text{av}} = 0$ at isotropic stresses, $\bar{Y}^{\text{av}} = 1$ at critical stress ratio). The underlying equations of the functions $f_{\sqcup}$ can be found in (Niemunis et al., 2005). They have been derived from an extensive laboratory testing program, which is documented in (Wichtmann, 2005; Wichtmann, 2016). The HCA model can be used to investigate the influence of the pile installation process on the response to large numbers of lateral load cycles if the state variables of soil at the start of the HCA analysis reflect the post installation state. This can be achieved by mapping the post installation state variables to a fully Lagrangian finite element model as is explained in the next section.

4.2 Numerical model for the lateral loading

As has been mentioned earlier, the finite element program `numgeo` is used to study the long-term behaviour of the piles following the installation process. A fully Lagrangian finite element model is used for the analysis of the high-cyclic loading since comparatively small deformations occur for which no large-deformation technique is required. For the soil, three-dimensional **u**-p finite elements with 27 nodes discretising the displacement **u** of the solid phase and 8 nodes discretising the pore water pressure p^w are utilised (termed `u27p8` element in `numgeo`). Hence, quadratic interpolation functions are used for the solid displacement while linear interpolation functions are applied for the pore water pressure (i.e. Taylor-Hood element formulation (Taylor and Hood, 1973)). The `u27p8` element is superior to the `u20p8` element in contact analyses as has been demonstrated in (Staubach et al., 2022a). The pile is modelled with single phase elements with 27 nodes (`u27`). The contact between soil and pile is discretised using a mortar contact discretisation technique, which implementation is discussed in detail in (Staubach et al., 2022d). A simple Coulomb friction model with the same parameters as applied for the simulation of the installation is applied.

The state variables (density/void ratio, effective stress and excess pore water pressure) of the soil at the end of the simulation of the installation are imported into the Lagrangian model by means of a nearest-neighbour search of the integration points of both models. For the pile installation simulations which did not reach the targeted embedment depth of 10 m (see Fig. 3), the spatial distribution is shifted by the missing penetration depth of 30 cm to achieve 10 m. The missing information of the soil state at the ground surface is obtained by assuming that it is identical to the state of the soil resulting from the installation at the top surface. The same mapping procedure as explained in (Heins and Grabe, 2017; Fan et al., 2021a; Staubach

et al., 2021c) is applied. Since the u27p8 elements have 27 integration points, the nearest-neighbour search is performed for every individual integration point. Note that the deformation of the soil is not transferred since it is believed to be insignificant compared to the influence of the installation-induced change in the soil state variables. In addition to previous studies, the excess pore water pressure is transferred to the Lagrangian model in case of the simulations of the installation process considering partially drained conditions. The consolidation process prior to the application of lateral loading is considered, since it is assumed that there is sufficient time between the end of the pile installation process and the start of the service of the structure for excess pore water pressures to dissipate. The lateral loading starts once hydrostatic conditions are reached. Note that the intergranular strain tensor, which is an internal variable of the hypoplastic model with intergranular strain extension accounting for the preceding small strain history, is not transferred. It changes rapidly during the installation process and its distribution depends on the current load phase of the pile driver (e.g. downwards or upwards directed cyclic movement of the vibrator). In addition, since the consolidation process following the installation is considered, the strain resulting from the dissipation of excess pore water pressure is believed to erase the small strain history of the installation process.

The adopted finite element model is given in Fig. 10. The field of pore water pressure following the installation by vibratory driving using a hydraulic conductivity of $k^w = 10^{-3}$ m/s is shown as an example. In addition to simulations incorporating the installation-induced soil changes, so-called wished-in-place (WIP) simulations are also performed, for which a constant distribution of density, a K_0 stress state and a hydrostatic pore water pressure distribution are assumed as initial state.

The characteristics of the (high-cyclic) lateral loading phase following the installation process are identical for all considered specifications of the installation. The following steps are performed:

1. Following the transfer of the void ratio, the effective stress and, if applicable, the excess pore water pressure, the soil-pile system is allowed to deform such that static force equilibrium is achieved. This is necessary since the system is not in static force equilibrium at the end of the installation process. As a result, the soil shows a maximum of ≈ 5 mm of displacement in this calculation phase. For the WIP simulation, only the contact between pile and soil is initialized in this step.

2. For the simulations with partial drainage during installation, a consolidation analysis is performed prior to the loading of the pile. 10^4 s are considered, which is a sufficient time for dissipation of all excess pore pressure for both values of hydraulic conductivity ($k^w = 10^{-3}$ m/s and $k^w = 10^{-4}$ m/s). All subsequent steps are identical for all simulations.

3. The pile is loaded vertically with a magnitude of 3 MN, accounting for the weight of the structure carried by the pile. The magnitude is chosen such that, taking into account the differences in embedment length and assuming identical diameter, a 5-MW offshore wind turbine exerting a weight of 1200 t and being embedded into the seabed by 40 m is considered, i.e. the weight is linearly scaled with respect to the different embedment lengths.

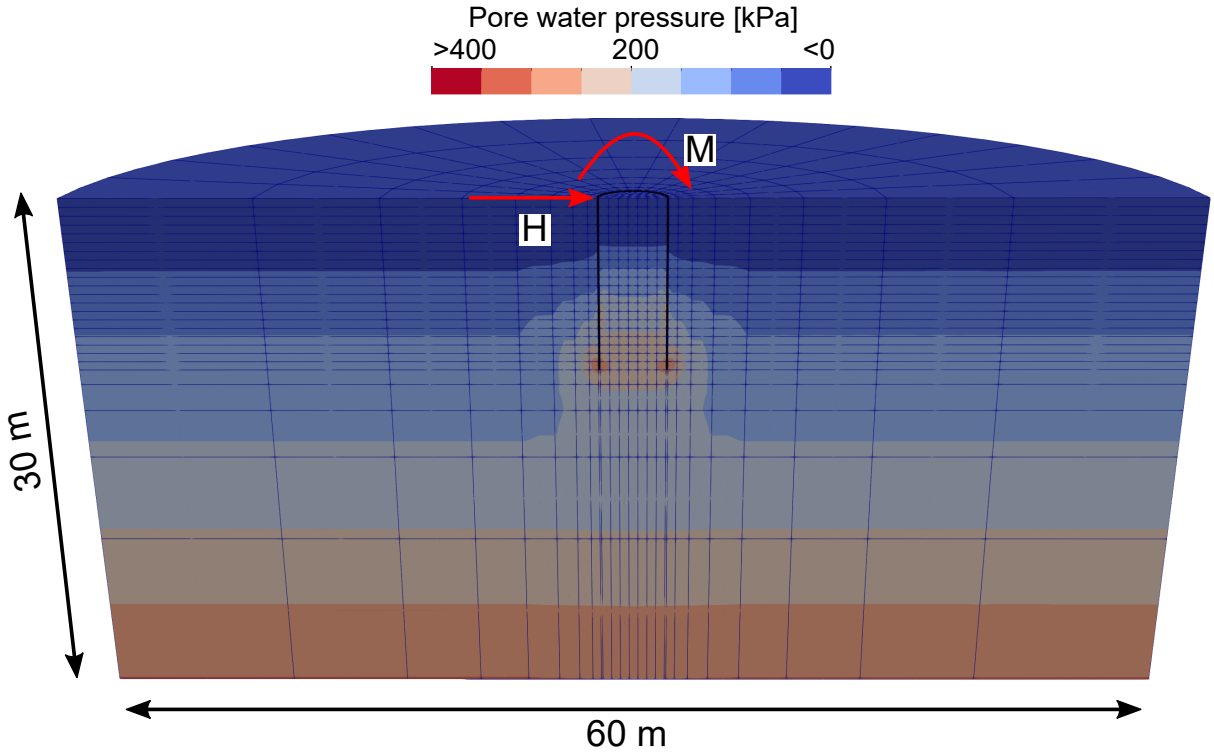

Fig. 10. Numerical model used for the analysis of the lateral loading of the pile following the installation process and transferred spatial distribution of pore water pressure following the installation by vibratory pile driving using a hydraulic conductivity of $k^w = 10^{-3}$ m/s. Note that only the nodes at the corners of the finite elements are visible.

4. Application of the mean value of horizontal loading, which is set to $H_{\mathrm{av}} = 200$ kN, and a mean value of moment $M_{\mathrm{av}} = 4.8$ MNm, both applied at the mudline (all loads for a full 3D model). The lever arm is thus 24 m. The magnitude of the load is chosen based on the monotonic load capacity of the piles, which is discussed in more detail on the basis of Fig. 11 later. The mean value of moment for the cyclic loading amounts approximately 10 % of the moment obtained at a pile head rotation of 1° for the pile with the largest moment resistance (i.e. the impact driven pile assuming ideally drained conditions). This and all following steps are performed assuming ideally drained conditions in order to investigate the influence of the different conditions during the pile installation process alone.

5. Application of the first load cycle with a horizontal load amplitude $H_{\mathrm{ampl}} = 200$ kN and a moment amplitude of $M_{\mathrm{ampl}} = 4.8$ MNm. Since the simulations are performed ideally drained and no inertia effects are considered, the rate of loading can be chosen arbitrarily (as long as the increment size is small enough to adequately capture the path-dependency of the constitutive model).

6. Repetition of the previous step while the strain path in every integration point is recorded. Based on this strain path the strain amplitude is calculated at the end of the step.

7. Simulation of 10^6 additional load cycles using the HCA model applying only the average loading H_{av} and M_{av}.

C_{ampl}	C_e	C_p	C_Y	C_{N1}	C_{N2}	C_{N3}
1.33	0.60	0.23	1.68	$2.95{\cdot}10^{-4}$	0.41	$1.9 \cdot 10^{-5}$

Table 3. Parameters of the HCA model for "Karlsruhe Fine Sand" (Source: Data from Wichtmann, 2016)

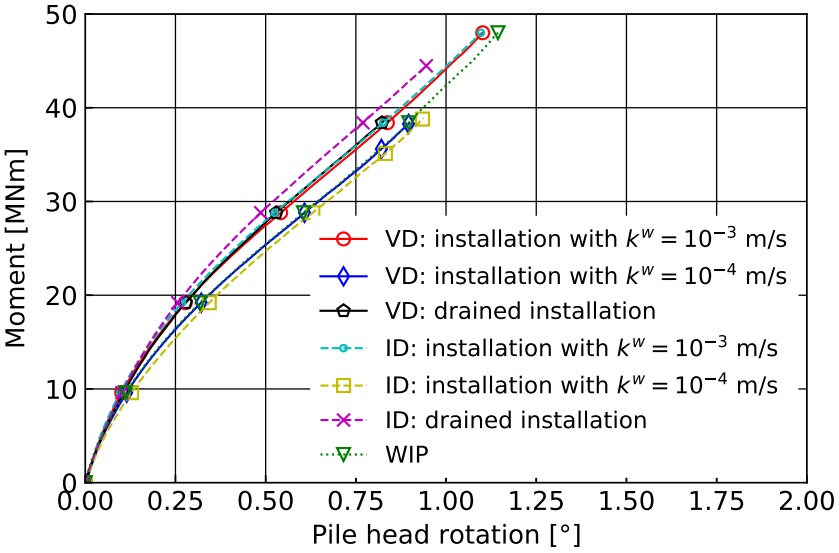

Fig. 11. Results of the simulations with monotonic lateral loading of the pile. The moment vs. pile head rotation for the vibratory (VD) and impact driven (ID) piles using different values of hydraulic conductivity as well as ideally drained conditions during the installation is presented. In addition, the results of a simulation without consideration of the installation process (WIP) are shown. Note that not all simulations reached 1° of pile head rotation due to non-convergence.

In analogy to the simulation of the installation process, the hypoplastic model with intergranular strain extension and the parameters of "Karlsruhe fine sand" provided in Table 1 are utilised for the first six steps. The parameters of the HCA model for "Karlsruhe Fine Sand" given in Table 3 are applied in the last step. During the simulation of the 10^6 cycles the strain amplitude is assumed constant. Previous studies using the adaptive strain amplitude definition proposed in (Staubach et al., 2022a) proved that for cyclic loading under drained conditions the strain amplitude remains approximately unchanged.

Prior to the simulations considering high-cyclic loading, a monotonic loading test is performed to determine the maximum moment resistance of the pile for each configuration, using the numerical model described earlier. Only the steps 1-4 are performed, but the horizontal force and the moment are linearly increased until a rotation at the pile head of 1° is reached in step 4. The results of the monotonic loading tests are given in Fig. 11. Note that only the simulations with initially dense soil conditions ($D_{r0} = 70$ %) are considered.

The simulations following the installation assuming ideally drained conditions result in the highest resistance of the pile. This is true for both installation techniques, but the impact driven pile exhibits a slightly larger stiffness compared to the vibratory driven pile. These trends do not necessarily contradict the findings from the spatial distributions shown and discussed on the basis of Fig. 5, where the vibratory

driven pile showed slightly stronger compaction of the soil close to the pile shaft, since the effective radial stress was less for the vibratory driven pile at the same time. With decreasing hydraulic conductivity during the installation, the resistance of the pile to subsequent lateral loading decreases, being slightly more pronounced for the impact driven piles. The assumption of WIP conditions results in a lower lateral capacity than obtained for drained vibratory or impact driven piles. Accounting for the effects of the coupled pore fluid-stress response during the installation leads to a lateral response comparable to that of a WIP pile. Overall though the influence of the installation process on the monotonic pile response is less significant for the high ratio of pile diameter and wall thickness D/t considered here than in cases with lower D/t (for simulations with lower ratio D/t see (Staubach et al., 2020b; Staubach et al., 2021a; Bienen et al., 2021; Le et al., 2021; Fan et al., 2021a)). Therefore, the assumption of WIP conditions for piles with a larger D/t ratio, such as for instance applied by recent numerical studies reported e.g. in (Burd et al., 2020; Hu et al., 2021), seems to be justified for the specifications considered in the present investigation. However, this conclusion does certainly depend on many different influencing factors (initial density, type of soil, etc.) in addition to the D/t ratio and is not believed to be generally applicable.

It is worth mentioning that a numerical study on the response of vibratory and impact driven piles to subsequent monotonic loading reported in (Heins and Grabe, 2017) also did not find significant differences between the two installation techniques regarding the response to lateral monotonic loading. Ideally drained behaviour was assumed during the pile installation process in that study. However, compared to the results presented in this work, no h/R effect was observed in case of impact driving.

4.3 Results of the simulations of high-cyclic loading following the installation

4.3.1 Initially dense soil ($D_{r0} = 70$ %)

The left-hand plot of Fig. 12 displays the pile head rotation with respect to the number of applied load cycles for the vibratory driven piles assuming partially drained conditions with different values of hydraulic conductivity or ideally drained conditions. The results of a WIP simulation are also provided for comparison.

As expected from the installation-induced soil changes discussed in Section 3.2, the drainage conditions during the installation process influence the subsequent response to the high-cyclic lateral loading considerably. The better the drainage during the installation, the lower are the accumulated pile head rotations after the application of one million load cycles. This is mainly attributed to the higher degree of compaction of the soil if the water can dissipate faster during the installation process.

Very similar observations are made for the impact driven piles, as is visible from the right-hand plot of Fig. 12. Interestingly, assuming ideally drained conditions the impact driven pile shows a larger permanent pile head rotation after $N = 10^6$ cycles compared to the corresponding vibratory driven pile. This does not necessarily contradict the results of the monotonic loading tests, where for larger values of pile head rotation the drained impact driven pile showed the largest resistance, since for the magnitude of the

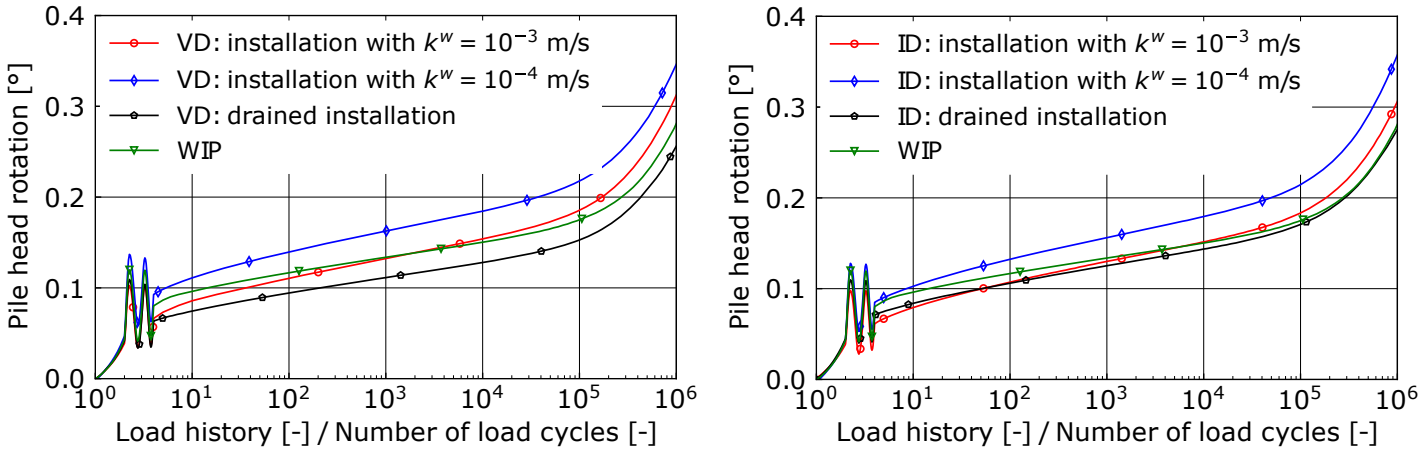

Fig. 12. Pile head rotation with respect to the number of load cycles for vibratory (VD) and impact driven (ID) piles assuming partially drained conditions with different values of hydraulic conductivity or ideally drained conditions during the installation. In addition, the results of a simulation without consideration of the installation process (WIP) are displayed.

cyclic load the drained impact driven pile does not give the lowest rotation (see Fig. 11). In addition, the tendencies observed from the monotonic loading are in general not necessarily transferable to cyclic loading. This is in particular the case for the present simulations, since two different constitutive models (Hypoplasticity with intergranular strain and the HCA model) are used, for which differences in soil state variables caused by the installation may (quantitatively) lead to different responses of the pile (e.g. the change in density due to the installation has a larger influence for one constitutive model than the other). The lower accumulation of pile head rotation of the vibratory driven pile assuming ideally drained conditions compared to the corresponding impact driven pile is in line with the field of relative density given in Fig. 5, where the vibratory driven pile showed stronger compaction of the soil near the pile tip compared to the impact driven pile. This explains why in the numerical analyses reported in (Le et al., 2021) vibratory driven piles are reported to show a lower accumulation of deformation compared to impact driven piles, since the simulation of the installation has been performed ideally drained. Similarly, a higher stiffness to lateral monotonic loading of vibratory driven piles compared to impact driven piles observed in the field test campaign reported in (Anusic et al., 2019) can be explained by the stronger compaction occurring without the presence of pore water.

The assumption of WIP conditions leads to comparable pile head rotations as the simulations considering the installation process, in particular if the installation is performed ideally drained or with a hydraulic conductivity of $k^w = 10^{-3}$ m/s. Compared to these two conditions, a lower accumulation rate for a larger number of load cycles is found for the WIP simulation, while the pile head rotation is larger at $N = 2$.

Assuming partially drained conditions with a hydraulic conductivity of $k^w = 10^{-3}$ m/s or $k^w = 10^{-4}$ m/s during the installation process, the vibratory driven piles tend to show a slightly higher rotation at the beginning of the high-cycle phase compared to the impact driven piles. However, at $N = 10^6$ cycles similar pile head rotations are obtained for both the vibratory and the impact driven piles. These results have to

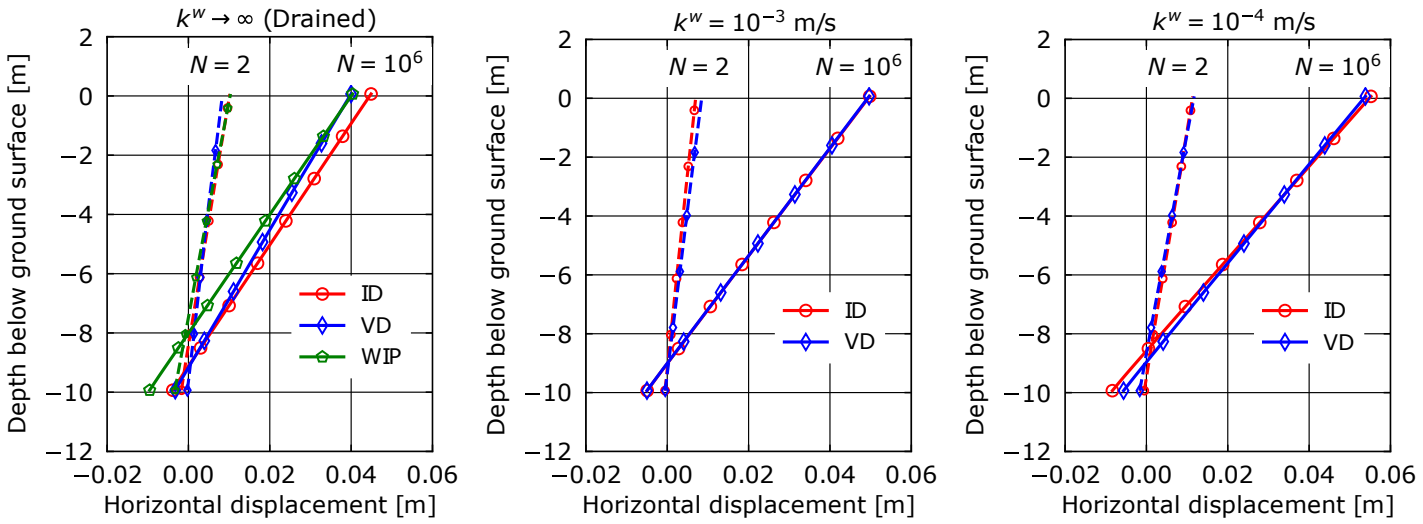

Fig. 13. Lateral deflection lines for vibratory (VD) and impact driven (ID) piles at $N = 2$ and at $N = 10^6$ cycles assuming different values of hydraulic conductivity as well as ideally drained conditions during the installation. In addition, the results of a simulation without consideration of the installation process (WIP) are displayed.

be interpreted keeping in mind that the pile penetration rate of the vibratory driven piles is slightly lower than the one of the impact driven piles. Since the drainage conditions during driving show a considerable influence on the response to subsequent loading, the differences in the pile penetration rate might also cause the impact driven piles to show more lateral deformations relative to the vibratory driven piles.

To better illustrate the differences in the pile behaviour due to the different initial conditions, the lateral deflection lines at $N = 2$ and at $N = 10^6$ cycles are shown in Fig. 13. In agreement with previous research (Staubach et al., 2020b), the consideration of the installation process results in a deeper position of the point of rotation (zero horizontal displacement) regardless of the number of load cycles, the installation technique, and the drainage conditions. This indicates that the pile installation decreases the soil stiffness near the ground surface while it is increased close to the pile tip. These trends are consistent with the spatial distributions of effective radial stress and relative density after the pile installation process discussed in Section 3.2. Fig. 13 also shows that there is no clear trend for the influence of the installation technique, as it depends on the drainage conditions during driving. As already discussed earlier, the vibratory driven pile exhibits less deflection in case of ideally drained conditions during driving. The influence of the installation technique is less for the partially drained conditions, in particular for $N = 10^6$ cycles. Similar observations have been made in the 1g small-scale model tests reported in (Hoffmann et al., 2020), where piles have been subjected to $N = 10^3$ lateral load cycles following impact and vibratory pile driving in water-saturated sand (initial relative density of approximately 75 % and hydraulic conductivity of approximately $5 \cdot 10^{-4}$ m/s).

The spatial distributions of the strain amplitude calculated based on the recorded strain path during the second load cycle are given in Fig. 14 for the vibratory driven pile ($k^w = 10^{-3}$ m/s) and the WIP simulation. In accordance with a preceding study on piles with a large L/D ratio reported in (Staubach

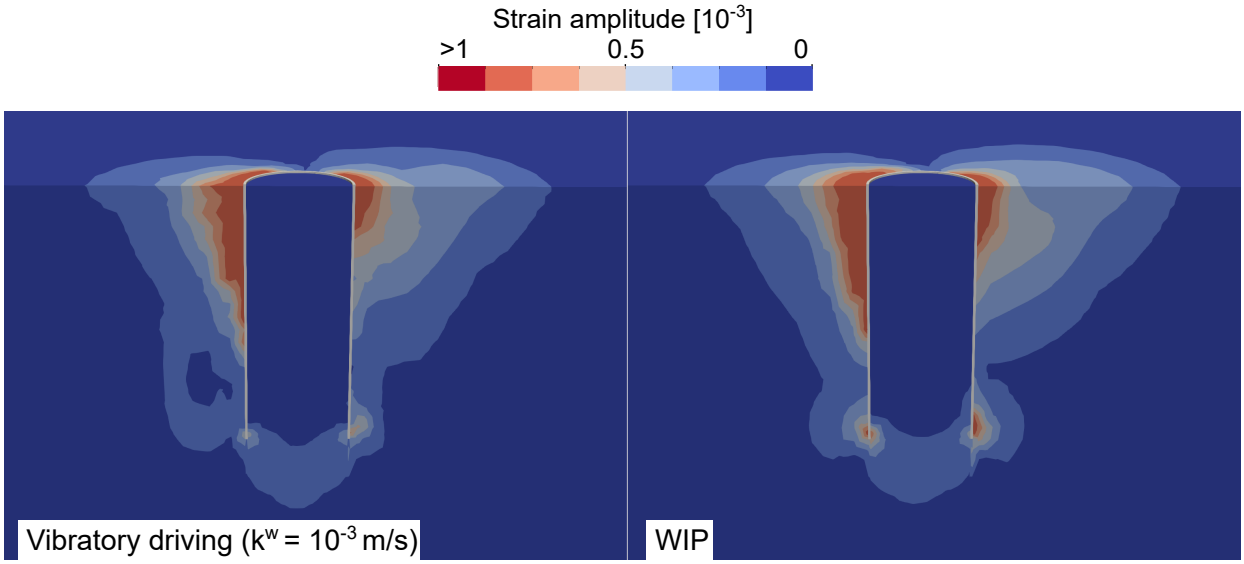

Fig. 14. Spatial distribution of the strain amplitude recorded from the second load cycle for the vibratory driven pile ($k^w = 10^{-3}$ m/s) and the WIP simulation, respectively

et al., 2020b), the consideration of the installation process results in lower values of the strain amplitude close to the pile tip. This is due to the increased stiffness resulting from the effective stress increase and compaction caused by the installation process. Around the pile head, however, the distributions are similar for both simulations.

The fields of relative density and horizontal effective stress after the application of one million load cycles are depicted in Fig. 15 for the vibratory driven pile ($k^w = 10^{-3}$ m/s) and the WIP simulation. Despite being initially dense, the soil around the outer pile head tends to compact due to the cyclic loading in both simulations. In case of the vibratory driven pile the alteration of the field of relative density caused by the installation process is still very well visible. As has been demonstrated in (Staubach et al., 2020b), an assimilation of the fields of relative density of the simulations incorporating and neglecting the installation occurs with increasing number of cycles, which eventually leads to similar accumulation rates for both simulation types. Thus, with ongoing cyclic loading, the influence of installation-induced changes in relative density reduces. The distribution of effective horizontal stress is similar for both initial conditions at $N = 10^6$, with both piles showing a reduction in effective stress where the soil is unloaded due to the lateral loading (left upper and right lower part of the pile). An increased effective horizontal stress below the pile tip is observed for both simulations.

4.3.2 Initially medium dense soil ($D_{r0} = 50$ %)

Previous research has found a large influence of the initial relative density of the soil prior to the installation process on the differences between simulations that neglect installation and those considering it (Staubach et al., 2020b; Fan et al., 2021a). However, these studies were limited to ideally drained conditions and to either impact driven or jacked piles. To investigate how the pile installation process affects the pile response to cyclic lateral loading in medium dense sand, additional simulations of the installation process

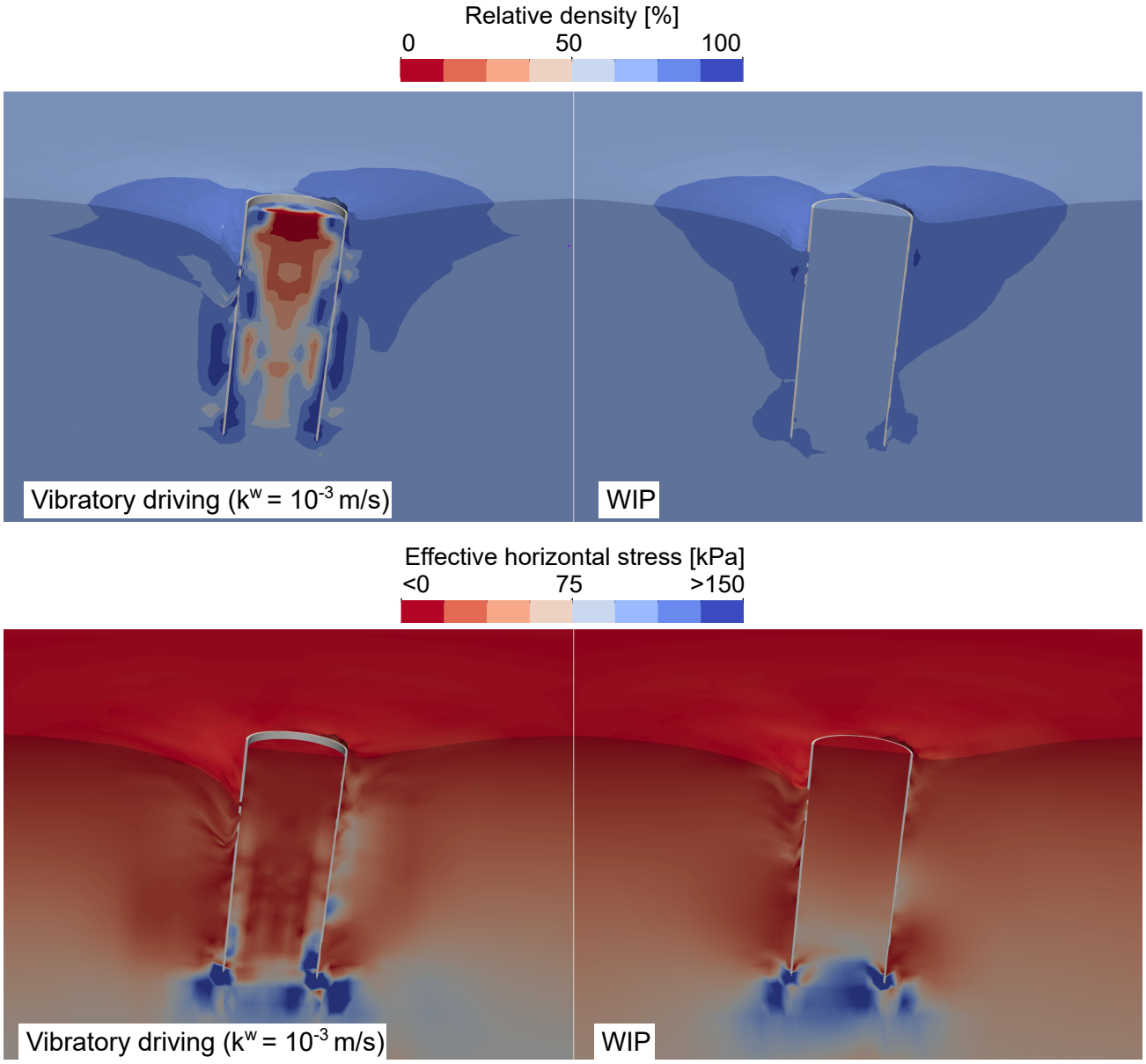

Fig. 15. Spatial distribution of relative density and the effective horizontal stress for the vibratory driven pile ($k^w = 10^{-3}$ m/s) and the WIP simulation after application of 10^6 lateral load cycles, respectively. The deformed configuration with a scale factor of 20 is displayed.

are performed with an initial relative density of $D_{r0} = 50$ % and assuming a hydraulic conductivity of $k^w = 10^{-3}$ m/s. To achieve pile penetration rates similar to the $D_{r0} = 70$ % case, both the impact load and the force amplitude of the vibratory driver are scaled by 2/3. With this loading, approximately 25 s are required to achieve a penetration of 10 m for both installation techniques. The spatial distributions of the state variables following the installation process are similar to those in case of initially dense soil conditions, but the compaction of the sand is generally greater and the effective radial stress close to the pile tip less. Slightly larger excess pore water pressures develop in addition. Following the installation process, the piles were subjected to the same cyclic loading as for the case with $D_{r0} = 70$ %. The resulting curves of pile head rotation vs. number of load cycles are shown in Fig. 16 for an impact driven (ID), a vibratory driven (VD) and a WIP pile. Note that in the case of the WIP pile, a homogeneous initial

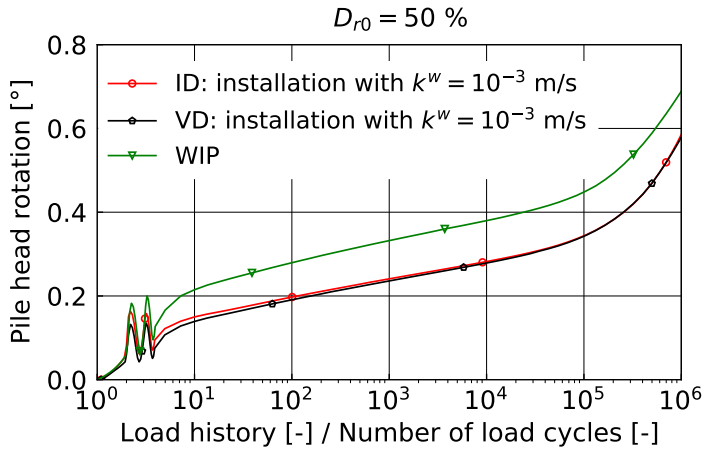

Fig. 16. Pile head rotation as a function of the number of load cycles for vibratory (VD) and impact driven (ID) piles assuming a hydraulic conductivity of $k^w = 10^{-3}$ m/s and an initial relative density of $D_{r0} = 50$ % prior to installation. In addition, the results of a simulation without consideration of the installation process (WIP) are displayed.

relative density of $D_{r0} = 50$ % is assumed. Consistent with previous research (Staubach et al., 2020b), the assumption of WIP conditions in case of initially medium dense soil results in higher accumulated pile deformations compared to the simulations that consider the installation process. A stronger influence of the consideration of the installation process compared to the initially dense condition is found. In line with the observations for $D_{r0} = 70$ %, the differences between the two studied installation methods are found to be rather small, with the impact driven pile showing slightly larger pile head rotations at low numbers of lateral load cycles.

5 Conclusions

The installation process changes the soil state in the vicinity of the pile considerably. The numerical analysis of vibratory or impact driven piles in water-saturated dense sand using a Coupled Eulerian-Lagrangian method indicated that the effective stress in the soil close to the pile tip is larger for the impact driven pile. A stronger increase of excess pore water pressure was observed for the vibratory driven pile. In line with these observations, the vibratory driven pile showed less densification in the soil close to the pile for partially drained conditions. However, if ideally drained conditions were assumed, the vibratory driven piles showed stronger compaction of the soil close to the pile tip compared to impact driven piles. For both installation techniques the h/R effect, i.e. decreasing effective radial stress with increasing distance h from the pile tip, has been observed. Close to the pile shaft the effective stress was comparable for both installation techniques, but in case of the impact driven piles the soil in greater distance showed larger effective radial stress in case of a hydraulic conductivity of the soil of $k^w = 10^{-3}$ m/s. Unsurprisingly, the lower the hydraulic conductivity of the soil, the higher was the excess pore water pressure and the less the compaction of the soil close to the pile tip. However, in greater distance from the pile shaft, the radial

effective stress was found to be larger for lower values of hydraulic conductivity due to the development of negative excess pore water pressure.

Following the installation process, the lateral high-cyclic loading of the pile, representing wind and water load faced by offshore pile foundations, was simulated using the high-cycle accumulation (HCA) model. The permanent pile head rotations after one million loading cycles were comparable for both impact and vibratory driven piles, if the hydraulic conductivity of the soil was $k^w = 10^{-3}$ m/s or $k^w = 10^{-4}$ m/s. However, if the installation was simulated assuming ideally drained conditions, the vibratory driven pile showed less pile head rotation after one million lateral load cycles, which was traced back to greater compaction of the soil caused by the installation process compared to the impact driven pile. For a lower hydraulic conductivity of $k^w = 10^{-4}$ m/s the lateral deformation of the pile was larger compared to $k^w = 10^{-3}$ m/s for both installation techniques. In general, the better the drainage during driving, the less pile head rotation occurred during the high-cyclic loading following the installation process.

The results of the study indicate that both installation techniques, vibratory and impact driving, result in comparable long-term deformations if the pile is subjected to high-cyclic lateral loading after the installation. It should be noted, however, that these results clearly depend on a variety of influencing factors and no general rule can be concluded yet. In addition, the study considered only rather simple initial conditions of the soil before installation (one soil layer, homogeneous distribution of relative density). Future work should investigate whether the conclusions drawn also apply to more complex initial conditions.

Data availability statement

Some or all data, models, or code that support the findings of this study are available from the corresponding author upon reasonable request. `numgeo` can be freely downloaded from www.numgeo.de.

References

Achmus, M., K. Schmoor, V. Herwig, and B. Matlock (Aug. 2020). "Lateral bearing behaviour of vibro- and impact-driven large-diameter piles in dense sand". In: *Geotechnik* 43.3, pp. 147–159. DOI: 10.1002/gete.202000006.

Andresen, L. and H. X. Khoa (2013). "LDFE analysis of installation effects for offshore anchors and foundations". In: *Installation Effects in Geotechnical Engineering*. Ed. by Hicks, pp. 162–168.

Anusic, I., B. M. Lehane, G. R. Eiksund, and M. A. Liingaard (2019). "Influence of installation method on static lateral response of displacement piles in sand". In: *Geotechnique Letters* 9.3, pp. 193–197. ISSN: 20452543. DOI: 10.1680/jgele.18.00191.

Argani, L. P. and A. Gajo (Nov. 2021). "A novel insight into vertical ground motion modelling in earthquake engineering". In: *International Journal for Numerical and Analytical Methods in Geomechanics*. ISSN: 0363-9061. DOI: https://doi.org/10.1002/nag.3295.

Aubram, D., F. Rackwitz, P. Wriggers, and S. A. Savidis (Apr. 2015). "An ALE method for penetration into sand utilizing optimization-based mesh motion". In: *Computers and Geotechnics* 65, pp. 241–249. ISSN: 18737633. DOI: 10.1016/j.compgeo.2014.12.012.

Augarde, C. E., S. J. Lee, and D. Loukidis (2021). "Numerical modelling of large deformation problems in geotechnical engineering: A state-of-the-art review". In: *Soils and Foundations*. ISSN: 0038-0806. DOI: https://doi.org/10.1016/j.sandf.2021.08.007.

Benson, D. J. (1992). "Computational methods in Lagrangian and Eulerian hydrocodes". In: *Computer Methods in Applied Mechanics and Engineering* 99.2, pp. 235–394. ISSN: 0045-7825.

Bienen, B., S. Fan, M. Schröder, and M. F. Randolph (Sept. 2021). "Effect of the installation process on monopile lateral response". In: *Proceedings of the Institution of Civil Engineers - Geotechnical Engineering*, pp. 1–19. ISSN: 1353-2618. DOI: 10.1680/jgeen.20.00219.

Bojanowski, C. (2014). "Numerical modeling of large deformations in soil structure interaction problems using FE, EFG, SPH, and MM-ALE formulations". In: *Archive of Applied Mechanics* 84.5, pp. 743–755. ISSN: 1432-0681. DOI: 10.1007/s00419-014-0830-5.

Bond, A. J. and R. J. Jardine (1991). "Effects of installing displacement piles in a high OCR clay". In: *Geotechnique* 41.3, pp. 341–363. ISSN: 17517656. DOI: 10.1680/geot.1991.41.3.341.

Burali d'Arezzo, F., S. Haigh, M. Talesnick, and Y. Ishihara (2015). "Measuring horizontal stresses during jacked pile installation". In: *Proceedings of the Institution of Civil Engineers - Geotechnical Engineering* 168.4, pp. 306–318.

Burd, H. J. et al. (Nov. 2020). "PISA design model for monopiles for offshore wind turbines: application to a marine sand". In: *Géotechnique* 70.11, pp. 1048–1066. ISSN: 0016-8505. DOI: 10.1680/jgeot.18.P.277.

Ceccato, F. and P. Simonini (2017). "Numerical study of partially drained penetration and pore pressure dissipation in piezocone test". In: *Acta Geotechnica* 12.1, pp. 195–209. ISSN: 18611133. DOI: 10.1007/s11440-016-0448-6.

Chow, F. C., R. J. Jardine, J. F. Nauroy, and F. Brucy (1997). "Time-related increases in the shaft capacities of driven piles in sand". In: *Geotechnique* 47.2, pp. 353–361. ISSN: 00168505. DOI: 10.1680/geot.1997.47.2.353.

Ciantia, M. O., M. Arroyo, J. Butlanska, and A. Gens (2016). "DEM modelling of cone penetration tests in a double-porosity crushable granular material". In: *Computers and Geotechnics* 73, pp. 109–127. ISSN: 18737633. DOI: 10.1016/j.compgeo.2015.12.001.

Cyril, P. A., S. T. Kok, M. K. Song, A. Chan, J. Y. Wong, and W. K. Choong (Aug. 2019). "Smooth particle hydrodynamics for the analysis of stresses in soil around Jack-in Pile". In: *European Journal of Environmental and Civil Engineering*, pp. 1–27. ISSN: 19648189. DOI: 10.1080/19648189.2019.1649198.

Dafalias, Y. F. and M. T. Manzari (2004). "Simple Plasticity Sand Model Accounting for Fabric Change Effects". In: *Journal of Engineering Mechanics* 130.6, pp. 622–634. ISSN: 0733-9399. DOI: 10.1061/(asce)0733-9399(2004)130:6(622).

DeJong, J. T., M. F. Randolph, and D. J. White (2003). "Interface load transfer degradation during cyclic loading: a microscale investigation". In: *Soils Found.* 43.4, pp. 81–93.

DeJong, J. T., D. J. White, and M. F. Randolph (Feb. 2006). "Microscale Observation and Modeling of Soil-Structure Interface Behavior Using Particle Image Velocimetry". In: *Soils and Foundations* 46.1, pp. 15–28. ISSN: 00380806. DOI: 10.3208/sandf.46.15.

DGGT (2012). *Empfehlungen des Arbeitskreises "Pfaehle" der Deutschen Gesellschaft für Geotechnik e.V., 2. Auflage.*

Dijkstra, J., W. Broere, and O. M. Heeres (2011). "Numerical simulation of pile installation". In: *Computers and Geotechnics* 38.5, pp. 612–622. ISSN: 0266-352X. DOI: https://doi.org/10.1016/j.compgeo.2011.04.004.

Dyson, G. J. and M. F. Randolph (2001). "Monotonic Lateral Loading of Piles in Calcareous Sand". In: *Journal of Geotechnical and Geoenvironmental Engineering* 127.4, pp. 346–352. DOI: 10.1061/(ASCE)1090-0241(2001)127:4(346).

Fan, S., B. Bienen, and M. F. Randolph (May 2021a). "Effects of Monopile Installation on Subsequent Lateral Response in Sand. II: Lateral Loading". In: *Journal of Geotechnical and Geoenvironmental Engineering* 147.5, p. 04021022. ISSN: 1090-0241. DOI: 10.1061/(ASCE)GT.1943-5606.0002504.

Fan, S., B. Bienen, and M. F. Randolph (2021b). "Centrifuge study on effect of installation method on lateral response of monopiles in sand". In: *International Journal of Physical Modelling in Geotechnics* 21.1, pp. 40–52. ISSN: 20426550. DOI: 10.1680/jphmg.19.00013.

Fan, S., B. Bienen, and M. F. Randolph (2021c). "Effects of Monopile Installation on Subsequent Lateral Response in Sand. I: Pile Installation". In: *Journal of Geotechnical and Geoenvironmental Engineering* 147.5, p. 04021021. ISSN: 1090-0241. DOI: 10.1061/(asce)gt.1943-5606.0002467.

Giridharan, S., S. Gowda, D. F. Stolle, and C. Moormann (2020). "Comparison of UBCSAND and Hypoplastic soil model predictions using the Material Point Method". In: *Soils and Foundations* 60.4, pp. 989–1000. ISSN: 00380806. DOI: 10.1016/j.sandf.2020.06.001.

Göttsche, K. M., U. Steinhagen, and P. M. Juhl (Dec. 2015). "Numerical evaluation of pile vibration and noise emission during offshore pile driving". In: *Applied Acoustics* 99, pp. 51–59. ISSN: 1872910X. DOI: 10.1016/j.apacoust.2015.05.008.

Grabe, J. and T. Pucker (2015). "Improvement of bearing capacity of vibratory driven open-ended tubular piles". In: *Frontiers in Offshore Geotechnics III - Proceedings of the 3rd International Symposium on Frontiers in Offshore Geotechnics, ISFOG 2015*, pp. 551–556. ISBN: 9781138028500. DOI: 10.1201/b18442-70.

Hamad, F. (2016). "Formulation of the axisymmetric CPDI with application to pile driving in sand". In: *Computers and Geotechnics* 74, pp. 141–150. ISSN: 18737633. DOI: 10.1016/j.compgeo.2016.01.003.

Hamann, T. (2015). "Zur Modellierung wassergesättigter Böden unter dynamischer Belastung und großen Bodenverformungen am Beispiel der Pfahleinbringung". PhD thesis. Publications of the Institute of Geotechnical Engineering and Construction Management, University of Hamburg.

Hamann, T., G. Qiu, and J. Grabe (2015). "Application of a Coupled Eulerian-Lagrangian approach on pile installation problems under partially drained conditions". In: *Computers and Geotechnics* 63, pp. 279–290. ISSN: 0266-352X. DOI: https://doi.org/10.1016/j.compgeo.2014.10.006.

Hauser, L. and H. F. Schweiger (2021). "Numerical study on undrained cone penetration in structured soil using G-PFEM". In: *Computers and Geotechnics* 133, p. 104061. ISSN: 18737633. DOI: 10.1016/j.compgeo.2021.104061.

Heerema, E. P. (1978). "Predicting pile driveability: Heather as an illustration of the "friction fatigue" theory". In: *Society of Petroleum Engineers - SPE European Petroleum Conference 1978* 13, pp. 413–422. DOI: 10.2118/8084-ms.

Heins, E. and J. Grabe (2017). "Class-A-prediction of lateral pile deformation with respect to vibratory and impact pile driving". In: *Computers and Geotechnics* 86, pp. 108–119. ISSN: 18737633. DOI: 10.1016/j.compgeo.2017.01.007.

Henke, S. (2014). "Untersuchungen zur Pfropfenbildung infolge der Installation offener Profile in granularen Böden". Habilitation. Hamburg-Harburg: Veröffentlichungen des Instituts für Geotechnik und Baubetrieb.

Henke, S., M. Milatz, and J. Grabe (2011). "Numerical simulations of acoustic emissions due to offshore-pile installation". In: *PAMM* 11.1, pp. 629–630. DOI: https://doi.org/10.1002/pamm.201110304.

Hoffmann, B., J. Labenski, and C. Moormann (2020). "Effects of Vibratory Driving of Monopiles on Soil Conditions and Their Cyclic Lateral Load Bearing Behavior". In: *4th International Symposium on Frontiers in Offshore Geotechnics*. Vol. 49. 0, pp. 714–724.

Hu, Q., F. Han, M. Prezzi, R. Salgado, and M. Zhao (2021). "Lateral load response of large-diameter monopiles in sand". In: *Géotechnique* 0.0, pp. 1–16. ISSN: 0016-8505. DOI: 10.1680/jgeot.20.00002.

Jardine, R. J., B. T. Zhu, P. Foray, and Z. X. Yang (2013a). "Measurement of stresses around closed-ended displacement piles in sand". In: *Géotechnique* 63.1, pp. 1–17. DOI: 10.1680/geot.9.P.137.

Jardine, R. J., B. T. Zhu, P. Foray, and Z. X. Yang (2013b). "Interpretation of stress measurements made around closed-ended displacement piles in sand". In: *Geotechnique* 63.8, pp. 613–627. ISSN: 00168505. DOI: 10.1680/geot.9.P.138.

Jostad, H. P., B. M. Dahl, A. Page, N. Sivasithamparam, and H. Sturm (2020). "Evaluation of soil models for improved design of offshore wind turbine foundations in dense sand". In: *Geotechnique* 70.8, pp. 682–699. ISSN: 17517656. DOI: 10.1680/jgeot.19.TI.034.

Labenski, J. and C. Moormann (2019). "Lateral bearing behaviour of vibratory-driven monopiles: A modified p-y approach based on experimental observations of scaled model tests". In: *17th European Conference on Soil Mechanics and Geotechnical Engineering, ECSMGE 2019 - Proceedings* 2019-Septe, pp. 1867–1874. DOI: 10.32075/17ECSMGE-2019-0350.

Le, V. H., F. Remspecher, and F. Rackwitz (2021). "Development of numerical models for the long-term behaviour of monopile foundations under cyclic loading considering the installation effects". In: *Soil*

Dynamics and Earthquake Engineering 150, p. 106927. ISSN: 02677261. DOI: 10.1016/j.soildyn.2021.106927.

Li, L., W. Wu, M. Hesham El Naggar, G. Mei, and R. Liang (2019). "DEM analysis of the sand plug behavior during the installation process of open-ended pile". In: *Computers and Geotechnics* 109, pp. 23–33. ISSN: 0266-352X. DOI: https://doi.org/10.1016/j.compgeo.2019.01.014.

Liyanapathirana, D. S. (2009). "Arbitrary Lagrangian Eulerian based finite element analysis of cone penetration in soft clay". In: *Computers and Geotechnics* 36.5, pp. 851–860. ISSN: 0266352X. DOI: 10.1016/j.compgeo.2009.01.006.

Machaček, J., T. Wichtmann, H. Zachert, and T. Triantafyllidis (2018). "Long-term settlements of a ship lock: measurements vs. FE-prediction using a high cycle accumulation model". In: *Computers and Geotechnics* 97.5, pp. 222–232.

Machaček, J., P. Staubach, M. Tafili, H. Zachert, and T. Wichtmann (2021). "Investigation of three sophisticated constitutive soil models: From numerical formulations to element tests and the analysis of vibratory pile driving tests". In: *Computers and Geotechnics* 138, p. 104276. ISSN: 18737633. DOI: 10.1016/j.compgeo.2021.104276.

Machaček, J. (2020). *Contributions to the Numerical Modelling of Saturated and Unsaturated Soils*. Dissertation, Publications of the Institute of Soil Mechanics and Rock Mechanics, Karlsruhe Institute of Technology, Issue No. 187.

Martinelli, M. and V. Galavi (2021). "Investigation of the Material Point Method in the simulation of Cone Penetration Tests in dry sand". In: *Computers and Geotechnics* 130, p. 103923. ISSN: 18737633. DOI: 10.1016/j.compgeo.2020.103923.

Monforte, L., A. Gens, M. Arroyo, M. Mánica, and J. M. Carbonell (2021). "Analysis of cone penetration in brittle liquefiable soils". In: *Computers and Geotechnics* 134, p. 104123. ISSN: 18737633. DOI: 10.1016/j.compgeo.2021.104123.

Mortara, G. and A. Mangiola (2007). "Cyclic shear stress degradation and post-cyclic behaviour from sand-steel interface direct shear tests". In: *Canadian Geotechnical Journal* 44.7, pp. 739–752.

Navas, P., M. Molinos, M. M. Stickle, D. Manzanal, A. Yagüe, and M. Pastor (2021). "Explicit meshfree u-p-w solution of the dynamic Biot formulation at large strain". In: *Computational Particle Mechanics*. ISSN: 2196-4386. DOI: 10.1007/s40571-021-00436-8.

Niemunis, A., T. Wichtmann, and T. Triantafyllidis (2005). "A high-cycle accumulation model for sand". In: *Computers and Geotechnics* 32.4, pp. 245–263.

Niemunis, A. and I. Herle (1997). "Hypoplastic model for cohesionless soils with elastic strain range". In: *Mechanics of Cohesive-Frictional Materials* 2.4, pp. 279–299. ISSN: 10825010. DOI: 10.1002/(SICI)1099-1484(199710)2:4<279::AID-CFM29>3.0.CO;2-8.

Page, A. M., R. T. Klinkvort, S. Bayton, Y. Zhang, and H. P. Jostad (Jan. 2021). "A procedure for predicting the permanent rotation of monopiles in sand supporting offshore wind turbines". In: *Marine Structures* 75, p. 102813. ISSN: 09518339. DOI: 10.1016/j.marstruc.2020.102813.

Phuong, N. T., F. Tol, A. Elkadi, and A. Rohe (2014). "Modelling of pile installation using the material point method (MPM)". In: *Numerical Methods in Geotechnical Engineering*. Ed. by Hicks, Brinkgreve, and Rohe. DOI: 10.1201/b17017-50.

Qiu, G., S. Henke, and J. Grabe (2011). "Application of a Coupled Eulerian-Lagrangian Approach on Geomechanical Problems Involving Large Deformation". In: *Computers and Geotechnics* 38, pp. 30–39.

Randolph, M. and S. Gourvenec (July 2017). *Offshore geotechnical engineering*. CRC Press, pp. 1–528. ISBN: 9781351988919. DOI: 10.1201/9781315272474.

Simon, B. R., J. S.-S. Wu, O. C. Zienkiewicz, and D. K. Paul (1986). "Evaluation of u-w and u-pi finite element methods for the dynamic response of saturated porous media using one-dimensional models". In: *International Journal for Numerical and Analytical Methods in Geomechanics* 10.5, pp. 461–482. ISSN: 1096-9853. DOI: 10.1002/nag.1610100502.

Soga, K., E. Alonso, A. Yerro, K. Kumar, and S. Bandara (2016). "Trends in large-deformation analysis of landslide mass movements with particular emphasis on the material point method". In: *Geotechnique* 66.3, pp. 248–273. ISSN: 17517656. DOI: 10.1680/jgeot.15.LM.005.

Staubach, P. and J. Machaček (Aug. 2019). "Influence of relative acceleration in saturated sand: Analytical approach and simulation of vibratory pile driving tests". In: *Computers and Geotechnics* 112, pp. 173–184. ISSN: 0266352X. DOI: 10.1016/j.compgeo.2019.03.027.

Staubach, P., J. Machaček, R. Sharif, and T. Wichtmann (June 2021a). "Back-analysis of model tests on piles in sand subjected to long-term lateral cyclic loading: Impact of the pile installation and application of the HCA model". In: *Computers and Geotechnics* 134, p. 104018. ISSN: 0266352X. DOI: 10.1016/j.compgeo.2021.104018.

Staubach, P., J. Machaček, and T. Wichtmann (2020a). "Impact of the installation on the long-term behaviour of offshore wind turbine pile foundations". In: *4th International Symposium on Frontiers in Offshore Geotechnics,* Taylor & Francis Group, London, UK.

Staubach, P. (2022). "Contributions to the numerical modelling of pile installation processes and high-cyclic loading of soils". PhD Thesis. Publications of the Institute of Foundation Engineering and Soil Mechanics, Ruhr-University Bochum.

Staubach, P., J. Machaček, M. C. Moscoso, and T. Wichtmann (2020b). "Impact of the installation on the long-term cyclic behaviour of piles in sand: A numerical study". In: *Soil Dynamics and Earthquake Engineering* 138, p. 106223. ISSN: 02677261. DOI: 10.1016/j.soildyn.2020.106223.

Staubach, P., J. Machaček, J. Skowronek, and T. Wichtmann (Feb. 2021b). "Vibratory pile driving in water-saturated sand: Back-analysis of model tests using a hydro-mechanically coupled CEL method". In: *Soils and Foundations* 61.1, pp. 144–159. ISSN: 00380806. DOI: 10.1016/j.sandf.2020.11.005.

Staubach, P., J. Machaček, L. Tschirschky, and T. Wichtmann (Feb. 2022a). "Enhancement of a high-cycle accumulation model by an adaptive strain amplitude and its application to monopile foundations". In: *International Journal for Numerical and Analytical Methods in Geomechanics* 46.2, pp. 315–338. ISSN: 0363-9061. DOI: 10.1002/nag.3301.

Staubach, P. and T. Wichtmann (Aug. 2020). "Long-term deformations of monopile foundations for offshore wind turbines studied with a high-cycle accumulation model". In: *Computers and Geotechnics* 124, p. 103553. ISSN: 0266352X. DOI: 10.1016/j.compgeo.2020.103553.

Staubach, P., J. Machaček, M. Tafili, and T. Wichtmann (Mar. 2022b). "A high-cycle accumulation model for clay and its application to monopile foundations". In: *Acta Geotechnica* 17.3, pp. 677–698. ISSN: 1861-1125. DOI: 10.1007/s11440-021-01446-9.

Staubach, P., J. Machaček, and T. Wichtmann (Dec. 2021c). "Large-deformation analysis of pile installation with subsequent lateral loading: Sanisand vs. Hypoplasticity". In: *Soil Dynamics and Earthquake Engineering* 151, p. 106964. ISSN: 02677261. DOI: 10.1016/j.soildyn.2021.106964.

Staubach, P., J. Machaček, and T. Wichtmann (June 2022c). "Mortar contact discretisation methods incorporating interface models based on Hypoplasticity and Sanisand: Application to vibratory pile driving". In: *Computers and Geotechnics* 146, p. 104677. ISSN: 0266352X. DOI: 10.1016/j.compgeo.2022.104677.

Staubach, P., J. Machaček, and T. Wichtmann (May 2022d). "Novel approach to apply existing constitutive soil models to the modelling of interfaces". In: *International Journal for Numerical and Analytical Methods in Geomechanics* 46.7, pp. 1241–1271. ISSN: 0363-9061. DOI: 10.1002/nag.3344.

Stein, P., J. Gattermann, E. Daumlechner, N. Hinzmann, and J. Stahlmann (Nov. 2020). *ZykLaMP Großmaßstäbliche Modellversuche zur lateralen Tragfähigkeit offener Stahlrohrpfähle unter zyklischer Belastung bei verschiedenen Einbringverfahren*. Report. DOI: 10.2314/KXP:1757076905.

Taylor, C. and P. Hood (1973). "A numerical solution of the Navier-Stokes equations using the finite element technique". In: *Computers and Fluids* 1.1, pp. 73–100. ISSN: 00457930. DOI: 10.1016/0045-7930(73)90027-3.

The Overseas Coastal Area Development Institute of Japan (2002). *Technical Standards and Commentaries for Port and Harbour Facilities in Japan*. 3-2-4 Kasumigaseki, Chiyoda-ku, Tokyo, 100-0013, Japan.

Tolooiyan, A. and K. Gavin (2011). "Modelling the Cone Penetration Test in sand using Cavity Expansion and Arbitrary Lagrangian Eulerian Finite Element Methods". In: *Computers and Geotechnics* 38.4, pp. 482–490. ISSN: 0266352X. DOI: 10.1016/j.compgeo.2011.02.012.

Tsetas, A. et al. (2020). "Experimental identification of the dynamic behaviour of pile-soil system installed by means of three different pile-driving techniques". In: *Eurodyn 2020: XI International Conference on Structural Dynamics*, pp. 3005–3015. DOI: 10.47964/1120.9245.20367.

Tsouvalas, A. (2020). "Underwater Noise Emission Due to Offshore Pile Installation: A Review". In: *Energies* 13.12. ISSN: 1996-1073. DOI: 10.3390/en13123037.

UBA (2011). *Empfehlung von Lärmschutzwerten bei der Errichtung von Offshore-Windenergieanlagen (OWEA)*.

Wang, D., B. Bienen, M. Nazem, Y. Tian, J. Zheng, T. Pucker, and M. F. Randolph (Apr. 2015). "Large deformation finite element analyses in geotechnical engineering". In: *Computers and Geotechnics* 65, pp. 104–114. DOI: 10.1016/j.compgeo.2014.12.005.

White, D. J. and M. D. Bolton (2004). "Displacement and strain paths during plane-strain model pile installation in sand". In: *Géotechnique* 54.6, pp. 375–397. DOI: 10.1680/geot.2004.54.6.375.

White, D. J. and B. M. Lehane (2004). "Friction fatigue on displacement piles in sand". In: *Geotechnique* 54.10, pp. 645–658. ISSN: 00168505. DOI: 10.1680/geot.2004.54.10.645.

Wichtmann, T. (2005). *Explicit accumulation model for non-cohesive soils under cyclic loading*. PhD thesis, Publications of the Institute of Foundation Engineering and Soil Mechanics, Ruhr-University Bochum, Issue No. 38.

Wichtmann, T. (2016). *Soil Behaviour Under Cyclic Loading: Experimental Observations, Constitutive Description and Applications*. Habilitation, Institute of Soil Mechanics and Rock Mechanics, Karlsruhe Institute of Technology, Issue No. 181.

Wichtmann, T., J. Machaček, H. Zachert, and H. Günther (2018). "Validierung eines hochzyklischen Akkumulationsmodells anhand von Modellversuchen und Messungen an realen Bauwerken". In: *Bautechnik* 96.2.

Wolffersdorff, P.-A. von (1996). "A hypoplastic relation for granular materials with a predefined limit state surface". In: *Mechanics of Cohesive-Frictional Materials* 1, pp. 251–271.

Yang, Z., R. Jardine, B. Zhu, C. Tsuha, and P. Foray (2010). "Sand grain crushing and interface shearing during displacement pile installation in sand". In: *Géotechnique* 60.6, pp. 469–482. DOI: 10.1680/geot.2010.60.6.469.

Yang, Z. X., Y. Y. Gao, R. J. Jardine, W. B. Guo, and D. Wang (2020). "Large Deformation Finite-Element Simulation of Displacement-Pile Installation Experiments in Sand". In: *Journal of Geotechnical and Geoenvironmental Engineering* 146.6, p. 4020044. DOI: 10.1061/(ASCE)GT.1943-5606.0002271.

Zachert, H. (2015). *Zur Gebrauchstauglichkeit von Gründungen für Offshore-Windenergieanlagen*. Dissertation, Publications of the Institute of Soil Mechanics and Rock Mechanics, Karlsruhe Institute of Technology, Issue No. 180.

Zachert, H., T. Wichtmann, P. Kudella, T. Triantafyllidis, and U. Hartwig (2020). "Inspection of a high-cycle accumulation model for sand based on recalculations of a full-scale test on a gravity base foundation for offshore wind turbines". In: *Computers and Geotechnics* 126.10, p. 103727.

Zhang, W., J. qiang Zou, X. wei Zhang, W. hai Yuan, and W. Wu (Aug. 2021). "Interpretation of cone penetration test in clay with smoothed particle finite element method". In: *Acta Geotechnica* 16.8, pp. 2593–2607. ISSN: 18611133. DOI: 10.1007/s11440-021-01217-6.

Zienkiewicz, O. C., C. T. Chang, and P. Bettess (1980). "Drained, undrained, consolidating and dynamic behaviour assumptions in soils". In: *Geotechnique* 30.4, pp. 385–395.

Zienkiewicz, O. C. and T. Shiomi (1984). "Dynamic behaviour of saturated porous media: The generalized Biot formulation and its numerical solution". In: *International Journal for Numerical and Analytical Methods in Geomechanics* 8.1, pp. 71–96. ISSN: 1096-9853. DOI: 10.1002/nag.1610080106.